Early dysfunction and progressive degeneration of the subthalamic nucleus in mouse models of Huntington's disease

Jeremy F Atherton, Eileen L McIver, Matthew RM Mullen, David L Wokosin, D James Surmeier, Mark D Bevan*

Department of Physiology, Feinberg School of Medicine, Northwestern University, Chicago, United States

Abstract The subthalamic nucleus (STN) is an element of cortico-basal ganglia-thalamo-cortical circuitry critical for action suppression. In Huntington's disease (HD) action suppression is impaired, resembling the effects of STN lesioning or inactivation. To explore this potential linkage, the STN was studied in BAC transgenic and Q175 knock-in mouse models of HD. At <2 and 6 months of age autonomous STN activity was impaired due to activation of K_{ATP} channels. STN neurons exhibited prolonged NMDA receptor-mediated synaptic currents, caused by a deficit in glutamate uptake, and elevated mitochondrial oxidant stress, which was ameliorated by NMDA receptor antagonism. STN activity was rescued by NMDA receptor antagonism or the break down of hydrogen peroxide. At 12 months of age approximately 30% of STN neurons had been lost, as in HD. Together, these data argue that dysfunction within the STN is an early feature of HD that may contribute to its expression and course.
DOI: 10.7554/eLife.21616.001

Introduction

The basal ganglia are a network of subcortical brain nuclei that are critical for action selection and central to the expression of several psychomotor disorders (*Albin et al., 1989*; *Wichmann and DeLong, 1996*). Information flow from the cortex to the output nuclei of the basal ganglia occurs via three major pathways. The so-called direct pathway through the striatum promotes movement and 'rewarding' behavior through inhibition of GABAergic basal ganglia output (*Chevalier and Deniau, 1990*; *Kravitz et al., 2010*; *Kravitz and Kreitzer, 2012*). In contrast, the indirect pathway via the striatum, external globus pallidus and subthalamic nucleus (STN) and the hyperdirect pathway through the STN suppress the same processes through elevation of basal ganglia output (*Maurice et al., 1999*; *Tachibana et al., 2008*; *Kravitz et al., 2010*; *Kravitz and Kreitzer, 2012*). Indeed, interruption of the indirect and hyperdirect pathways through lesion or inactivation of the STN is associated with elevated/involuntary movement, impulsivity and psychiatric disturbances such as hypomania and hyper-sexuality (*Crossman et al., 1988*; *Hamada and DeLong, 1992*; *Baunez and Robbins, 1997*; *Bickel et al., 2010*; *Jahanshahi et al., 2015*).

Huntington's disease (HD) is an autosomal dominant, neurodegenerative disorder caused by an expansion of CAG repeats in the gene (*HTT*) encoding huntingtin (HTT), a protein involved in vesicle dynamics and intracellular transport (*Huntington's Disease Collaborative Research Group, 1993*; *Saudou and Humbert, 2016*). Early symptoms of HD include involuntary movement, compulsive behavior, paranoia, irritability and aggression (*Anderson and Marder, 2001*; *Kirkwood et al., 2001*). These symptoms have traditionally been linked to cortico-striatal degeneration, however a role for the STN is suggested by their similarity to those caused by STN inactivation or lesion. The hypoactivity of the STN in HD models in vivo (*Callahan and Abercrombie, 2015a*, *2015b*) and the

susceptibility of the STN to degeneration in HD (*Lange et al., 1976*; *Guo et al., 2012*) are also consistent with STN dysfunction.

Several mouse models of HD have been generated, which vary by length and species origin of *HTT/Htt*, CAG repeat length, and method of genome insertion. For example, one line expresses full-length human HTT with 97 mixed CAA-CAG repeats in a bacterial artificial chromosome (BAC; *Gray et al., 2008*), whereas Q175 knock-in (KI) mice have an inserted chimeric human/mouse exon one with a human polyproline region and ~188 CAG repeats in the native *Htt* (*Menalled et al., 2012*).

Increased mitochondrial oxidant stress exacerbated by abnormal NMDAR-mediated transmission and signaling has been reported in HD and its models (*Fan and Raymond, 2007*; *Song et al., 2011*; *Johri et al., 2013*; *Parsons and Raymond, 2014*; *Martin et al., 2015*). Several reports suggest that glutamate uptake is impaired due to reduced expression of the glutamate transporter EAAT2 (GLT-1) and/or GLT-1 dysfunction (*Arzberger et al., 1997*; *Liévens et al., 2001*; *Behrens et al., 2002*; *Miller et al., 2008*; *Bradford et al., 2009*; *Faideau et al., 2010*; *Huang et al., 2010*; *Menalled et al., 2012*; *Dvorzhak et al., 2016*; *Jiang et al., 2016*). However, others have found no evidence for deficient glutamate uptake (*Parsons et al., 2016*), suggesting that abnormal NMDAR-mediated transmission is caused by increased expression of extrasynaptic receptors and/or aberrant coupling to signaling pathways (e.g., *Parsons and Raymond, 2014*). The sensitivity of mitochondria to anomalous NMDAR signaling is likely to be further compounded by their intrinsically compromised status in HD (*Song et al., 2011*; *Johri et al., 2013*; *Martin et al., 2015*).

Although HD models exhibit pathogenic processes seen in HD, they do not exhibit similar levels and spatiotemporal patterns of cortico-striatal neurodegeneration. Striatal neuronal loss in aggressive *Htt* fragment models such as R6/2 mice does occur but only close to death (*Stack et al., 2005*), whereas full-length models exhibit minimal loss (*Gray et al., 2008*; *Smith et al., 2014*). Despite the loss and hypoactivity of STN neurons in HD and the similarity of HD symptoms to those arising from STN lesion or inactivation, the role of the STN in HD remains poorly understood. We hypothesized that the abnormal activity and progressive loss of STN neurons in HD may reflect abnormalities within the STN itself. This hypothesis was addressed in the BAC and Q175 KI HD models using a combination of cellular and synaptic electrophysiology, optogenetic interrogation, two-photon imaging and stereological cell counting.

Results

Data are reported as *median [interquartile range]*. Unpaired and paired statistical comparisons were made with non-parametric Mann-Whitney U and Wilcoxon Signed-Rank tests, respectively. Fisher's exact test was used for categorical data. $p < 0.05$ was considered statistically significant; where multiple comparisons were performed this p-value was adjusted using the Holm-Bonferroni method (adjusted p-values are denoted p_h; *Holm, 1979*). Box plots show median (central line), interquartile range (box) and 10–90% range (whiskers).

The autonomous activity of STN neurons is disrupted in the BACHD model

STN neurons exhibit intrinsic, autonomous firing, which contributes to their role as a driving force of neuronal activity in the basal ganglia (*Bevan and Wilson, 1999*; *Beurrier et al., 2000*; *Do and Bean, 2003*). To determine whether this property is compromised in HD mice, the autonomous activity of STN neurons in ex vivo brain slices prepared from BACHD and wild type littermate (WT) mice were compared using non-invasive, loose-seal, cell-attached patch clamp recordings. 5–7 months old, symptomatic and 1–2 months old, presymptomatic mice were studied (*Gray et al., 2008*). Recordings focused on the lateral two-thirds of the STN, which receives input from the motor cortex (*Kita and Kita, 2012*; *Chu et al., 2015*). At 5–7 months, 124/128 (97%) WT neurons exhibited autonomous activity compared to 110/126 (87%) BACHD neurons ($p = 0.0049$; *Figure 1A,B*). The frequency (WT: 7.9 [5.2–12.6] Hz; n = 128; BACHD: 6.3 [1.4–10.2] Hz; n = 126; $p = 0.0001$) and regularity (WT CV: 0.27 [0.14–0.47]; n = 124; BACHD CV: 0.36 [0.20–0.80]; n = 110; $p = 0.0012$) of firing were reduced in BACHD neurons (*Figure 1A,B*). The distribution of firing frequency of WT neurons appears unimodal with a mode at ~6–8 Hz (*Figure 1C*), whereas the distribution of BACHD neurons is relatively bimodal with modes at ~0–2 Hz and ~8–10 Hz (Kolmogorov–Smirnov test, $p = 0.0002$;
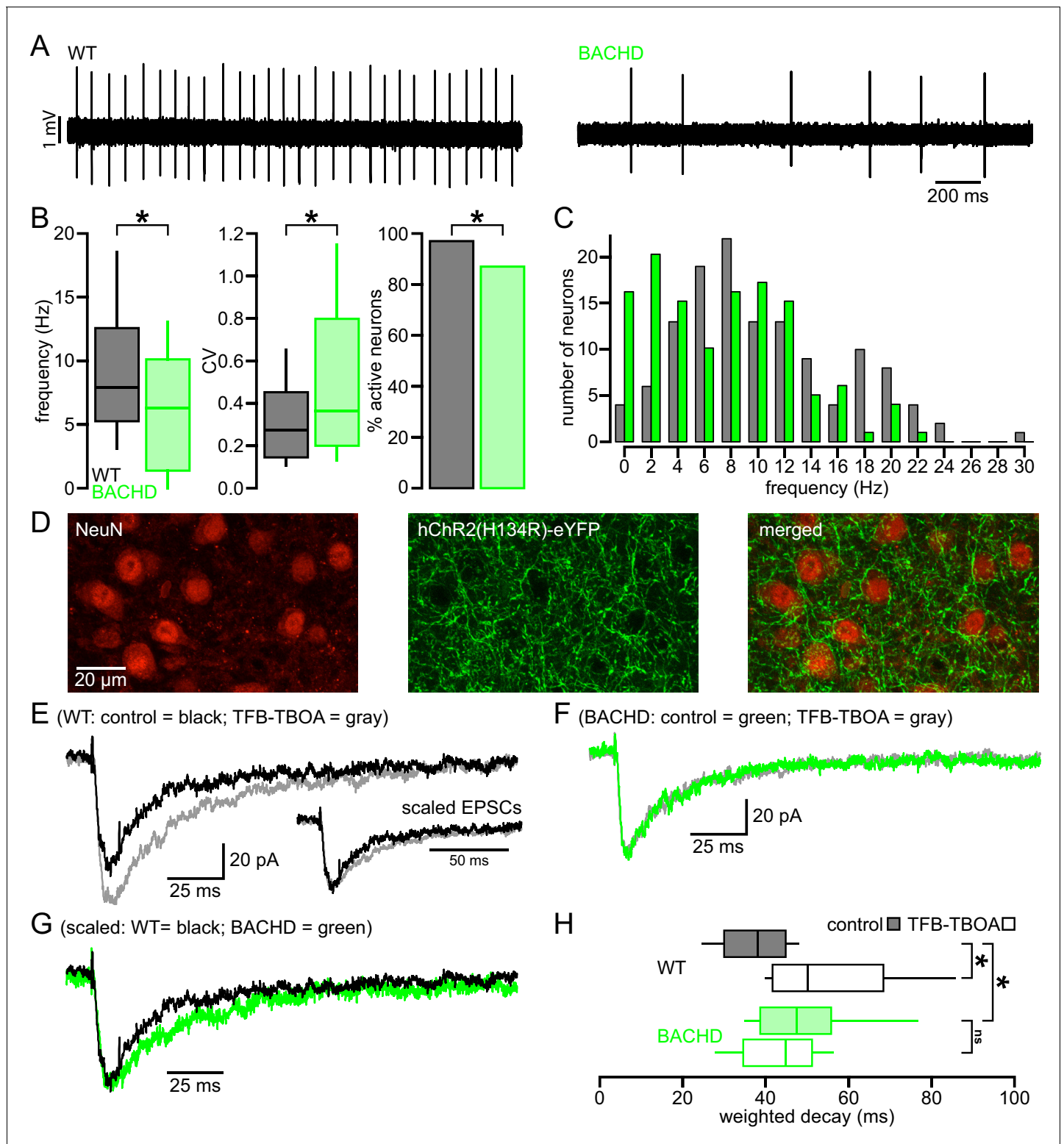
Figure 1. Abnormal intrinsic and synaptic properties of STN neurons in BACHD mice. (**A**) Representative examples of autonomous STN activity recorded in the loose-seal, cell-attached configuration. The firing of the neuron from a WT mouse was of a higher frequency and regularity than the phenotypic neuron from a BACHD mouse. (**B**) Population data showing (left to right) that the frequency and regularity of firing, and the proportion of active neurons in BACHD mice were reduced relative to WT mice. (**C**) Histogram showing the distribution of autonomous firing frequencies of neurons in WT (gray) and BACHD (green) mice. (**D**) Confocal micrographs showing NeuN expressing STN neurons (red) and hChR2(H134R)-eYFP expressing cortico-STN axon terminals (green) in the STN. (**E**) Examples of optogenetically stimulated NMDAR EPSCs from a WT STN neuron before (black) and

Figure 1 continued on next page

Figure 1 continued

after (gray) inhibition of astrocytic glutamate uptake with 100 nM TFB-TBOA. Inset, the same EPSCs scaled to the same amplitude. (F) Examples of optogenetically stimulated NMDAR EPSCs from a BACHD STN neuron before (green) and after (gray) inhibition of astrocytic glutamate uptake with 100 nM TFB-TBOA. (G) WT (black, same as in E) and BACHD (green, same as in F) optogenetically stimulated NMDAR EPSCs overlaid and scaled to the same amplitude. (H) Boxplots of amplitude weighted decay show slowed decay kinetics of NMDAR EPSCs in BACHD STN neurons compared to WT, and that TFB-TBOA increased weighted decay in WT but not BACHD mice. *p < 0.05. ns, not significant. Data for panels B–C provided in *Figure 1— source data 1*; data for panel H provided in *Figure 1—source data 2*.

Figure 1C). This distribution suggests that BACHD neurons consist of a phenotypic population with compromised autonomous firing, and a non-phenotypic population with relatively normal autonomous firing. At 1–2 months 136/145 (94%) WT STN neurons were autonomously active versus 120/143 (84%) BACHD STN neurons (p = 0.0086). The frequency (WT: 9.8 [6.3–14.8] Hz; n = 145; BACHD: 7.1 [1.8–11.3] Hz; n = 143; p < 0.0001) and regularity (WT CV: 0.17 [0.13–0.26]; n = 136; BACHD CV: 0.23 [0.14–0.76]; n = 120; p = 0.0016) of firing were also reduced in BACHD neurons. Together, these data demonstrate that the autonomous activity of STN neurons in BACHD mice is impaired at both early presymptomatic and later symptomatic ages.

NMDAR-mediated EPSCs are prolonged in BACHD STN neurons

As described above, the majority of studies report that astrocytic glutamate uptake is diminished in the striatum in HD and its models. To test whether the STN of BACHD mice exhibits a similar deficit, EPSCs arising from the optogenetic stimulation of motor cortical inputs to the STN (as described by *Chu et al., 2015*) were compared in WT and BACHD mice before and after inhibition of GLT-1 and GLAST with 100 nM TFB-TBOA. STN neurons were recorded in ex vivo brain slices in the whole-cell voltage-clamp configuration using a cesium-based, QX-314-containing internal solution to maximize voltage control. Neurons were held at −40 mV and recorded in the presence of low (0.1 mM) external Mg^{2+} and the AMPAR antagonist DNQX (20 μM) to maximize and pharmacologically isolate the evoked NMDAR-mediated excitatory postsynaptic current (EPSC); analysis was performed on average EPSCs from 5 trials with 30 s recovery between trials (*Figure 1D–H*). The amplitude weighted decay time constant of the NMDAR EPSC was moderately but significantly prolonged in BACHD compared to WT neurons (WT: 38.1 [30.0–44.8] ms; n = 12; BACHD: 47.6 [38.7–55.9] ms; n = 11; p = 0.0455; *Figure 1E–H*). Subsequent application of TFB-TBOA increased the decay time constant of the NMDAR EPSC in STN neurons derived from WT (WT control: 39.0 [35.2–44.0] ms; WT TFB-TBOA: 50.2 [41.7–68.4] ms; n = 9; p = 0.0039; *Figure 1E,H*) but had no effect in BACHD neurons (BACHD control: 47.9 [38.9–59.4] ms; BACHD TFB-TBOA: 44.9 [34.7–52.2] ms; n = 10; p = 0.3223; *Figure 1F,H*). In control conditions, the amplitudes of EPSCs recorded from WT and BACHD neurons were similar (WT: 50.1 [34.7–61.0] pA; n = 12; BACHD: 45.6 [22.1–78.3] pA; n = 11; p_h = 0.7399; *Figure 2A*) and there was no correlation between EPSC amplitude and the decay time constant in either group (WT: r^2 = 0.16; n = 12; p_h = 0.5871; BACHD: r^2 = 0.10; n = 12; p_h = 0.6686; *Figure 2B*). In order to increase spillover of glutamate from synaptic release sites, cortico-STN inputs were optogenetically stimulated 5 times at 50 Hz and the resulting compound NMDAR-mediated EPSC was compared in WT and BACHD STN neurons. Interestingly, the decay of compound NMDAR EPSCs under control conditions or following inhibition of glutamate uptake were not different in WT and BACHD mice (WT control: 79.0 [62.6–102.0] ms; n = 6; BACHD control: 65.2 [44.7–111.5] ms; n = 6; p = 0.4848; WT TFB-TBOA: 125.4 [106.8–146.6] ms; n = 6; BACHD TFB-TBOA: 108.3 [94.5–143.1] ms; n = 6; p = 0.6991; *Figure 2C–E*). Together, these data demonstrate that individual, but not compound, NMDAR-mediated cortico-STN synaptic EPSCs are prolonged in the BACHD model.
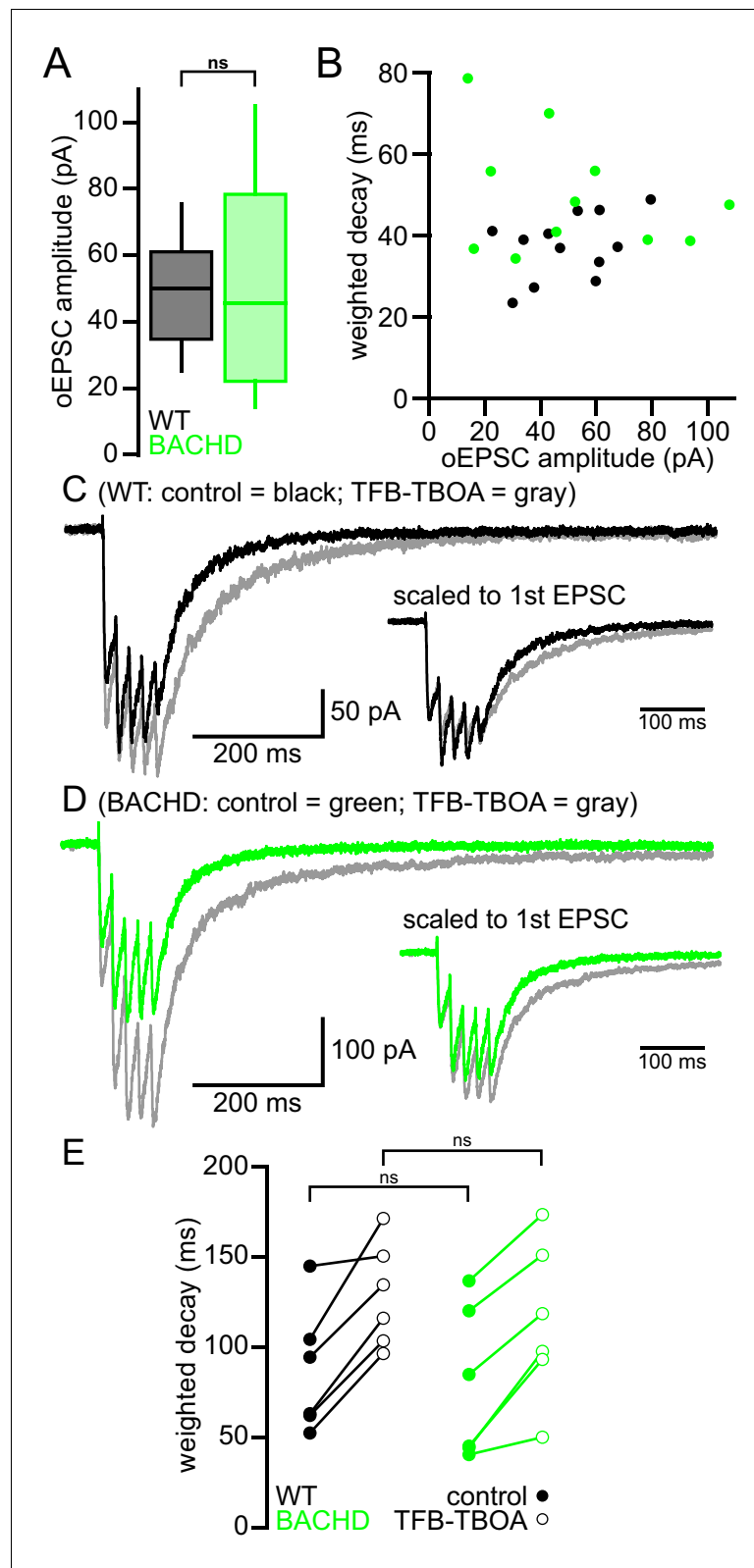
Figure 2. Cortico-STN EPSCs in WT and BACHD mice. (**A**) Boxplot showing the distribution of single optogenetically stimulated cortico-STN NMDAR EPSC amplitudes in WT and BACHD mice. (**B**) Scatterplot showing NMDAR EPSC amplitude vs amplitude weighted decay time. There was no correlation between NMDAR EPSC amplitude and decay time in WT or BACHD mice. (**C–D**) Example of NMDAR EPSCs generated by 5 × 50 Hz

Figure 2 continued on next page

Figure 2 continued

optogenetic stimulation from a WT STN neuron (C) before (black) and after (gray) inhibition of astrocytic glutamate uptake with 100 nM TFB-TBOA and a BACHD STN neuron (D) before (green) and after (gray) TFB-TBOA application. (E) Line segment plots of amplitude weighted decay of compound NMDAR EPSCs before and following TFB-TBOA. The decays of compound NMDAR ESPCs were similar in WT and BACHD before TFB-TBOA application. In addition, inhibition of astrocytic glutamate uptake prolonged the decay of compound NMDAR ESPCs in all neurons tested. ns, not significant. Data for panels A–B provided in *Figure 2—source data 1*; data for panel E provided in *Figure 2—source data 2*.

Blockade of NMDARs rescues the autonomous activity of BACHD STN neurons

To test whether disrupted autonomous firing in BACHD is linked to NMDAR activation, brain slices from BACHD mice were incubated in control media or media containing the NMDAR antagonist D-AP5 (50 μM) for 3–5 hr prior to loose-seal, cell-attached recordings from STN neurons (*Figure 3*). D-AP5 treatment rescued autonomous firing in slices derived from 5–7 month old BACHD mice compared to untreated control slices (*Figure 3A,B*). The proportion of autonomously active neurons was greater in D-AP5 pre-treated slices (untreated: 18/30 (60%); D-AP5 treated: 29/30 (97%); p = 0.0011). The frequency (untreated: 1.0 [0.0–7.6] Hz; n = 30; D-AP5 treated: 13.2 [7.9–17.4] Hz; n = 30; p < 0.0001) and regularity (untreated CV: 0.43 [0.24–1.21]; n = 18; D-AP5 treated: CV: 0.13 [0.09–0.20]; n = 29; p < 0.0001) of autonomous firing were also greater in D-AP5 treated slices. In slices derived from 1–2 month old BACHD mice autonomous firing was also more prevalent in D-AP5 treated slices than in untreated slices (untreated: 10/30 (33%); D-AP5-treated: 27/30 neurons (90%); p < 0.0001) and the frequency of firing overall was greater (untreated: 0.0 [0.0–1.3] Hz; n = 30; D-AP5 treated: 8.7 [4.4–14.5] Hz; n = 30; p < 0.0001; *Figure 3B*). The regularity of autonomous firing was however not rescued (untreated CV: 0.61 [0.27–0.81]; n = 10; D-AP5-treated CV: 0.25 [0.14–0.69]; n = 27; p = 0.1368; *Figure 3B*). In slices from WT mice the rate (untreated: 10.4 [6.1–14.2] Hz; n = 27; D-AP5 treated: 5.6 [1.7–15.4] Hz; n = 27; p = 0.1683; *Figure 3B*), regularity (untreated: 0.18 [0.12–0.27]; n = 24; D-AP5 treated: 0.22 [0.12–0.46]; n = 22; p = 0.4785; *Figure 3C*) and incidence of firing (untreated: 24/27 (89%); D-AP5 treated 22/27 (81%); p = 0.7040; *Figure 3D*) were unaltered by D-AP5 treatment. Thus, prolonged blockade of NMDARs rescued autonomous firing in BACHD STN neurons but had no effect on autonomous activity in WT STN neurons. Together, these data demonstrate that NMDAR activation contributes to the disruption of autonomous activity in BACHD STN neurons.

The mitochondria of BACHD STN neurons are subject to elevated oxidant stress

NMDAR activation can elevate mitochondrial oxidant stress (*Dugan et al., 1995*; *Moncada and Bolaños, 2006*; *Brennan et al., 2009*; *Nakamura and Lipton, 2011*). To test whether STN neurons from BACHD mice exhibit increased mitochondrial oxidant stress, a mitochondria-targeted redox probe MTS-roGFP (*Hanson et al., 2004*) was virally expressed in 5–7-month-old BACHD mice and WT littermates (*Figure 4A*). 1–2 weeks later MTS-roGFP was imaged in brain slices under two-photon excitation with 890 nm light. Oxidant stress was estimated from the fluorescence of MTS-roGFP in individual neurons under baseline conditions relative to the fluorescence of MTS-roGFP under conditions of full reduction and oxidation in the presence of 2 mM dithiothreitol and 200 μM aldrithiol-4, respectively (*Sanchez-Padilla et al., 2014*). STN neurons were selected for analysis based on their appearance under two-photon, Dodt contrast imaging and were distinguishable from STN glial cells by their relatively large diameter (*Figure 4A*). STN neurons are reliably recorded when this selection strategy is employed to guide patch clamp recording (*Atherton et al., 2008, 2010*). MTS-roGFP imaging revealed that relative oxidant stress in BACHD STN neurons was elevated compared
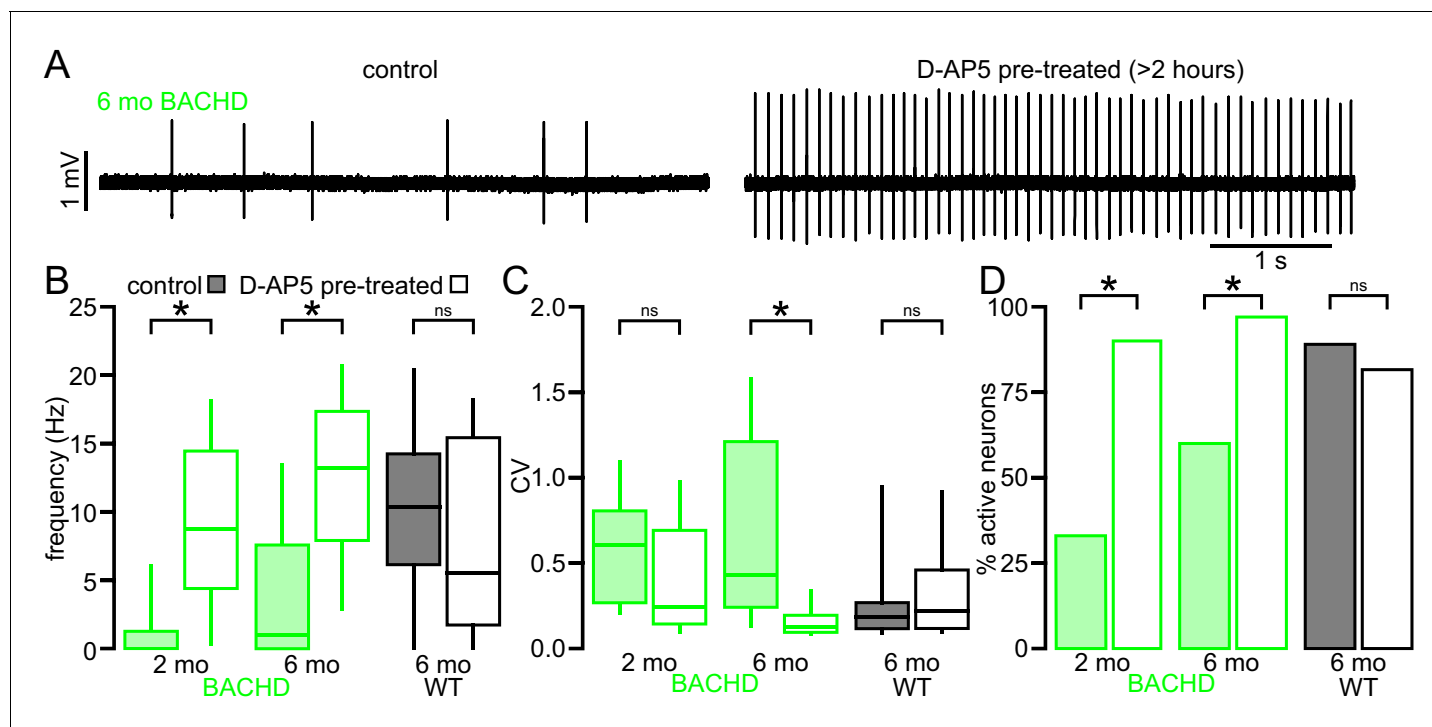
Figure 3. The impaired autonomous activity of STN neurons in BACHD mice is rescued by antagonism of NMDARs. (**A**) Examples of loose-seal cell-attached recordings of 6-month-old BACHD STN neurons from an untreated slice (left) and a slice that was treated with 50 µM D-AP5 for 3–5 hr prior to recording. (**B**) Population data showing elevated autonomous firing in STN neurons from D-AP5 pre-treated slices from 2-month-old and 6-month-old BACHD mice but not in WT mice. (**C**) Population data showing increased firing regularity in STN neurons from D-AP5 pre-treated slices from 6-month-old BACHD mice but not 2-month-old BACHD mice or WT mice. (**D**) Population data showing a higher proportion of active neurons in STN neurons from D-AP5 pre-treated slices from 2-month-old and 6-month-old BACHD mice but not in WT mice. *p < 0.05. ns, not significant. Data for panels B–C provided in *Figure 3—source data 1*.

DOI: 10.7554/eLife.21616.008

The following source data is available for figure 3:

Source data 1. Autonomous firing frequency and CV for BACHD control and D-AP5 pretreated STN neurons in *Figure 3B–C*.
DOI: 10.7554/eLife.21616.009

to WT (WT: 0.35 [0.18–0.42]; n = 23; BACHD: 0.40 [0.37–0.63]; n = 24; p = 0.0332; *Figure 4B*). In a separate experiment (performed 15 months later) to test whether NMDAR activation ex vivo contributed to elevated mitochondrial oxidant stress, brain slices from a different cohort of BACHD mice were treated for >3 hr in 50 µM D-AP5 prior to imaging. MTS-roGFP imaging confirmed that D-AP5-treated slices exhibited lower oxidant stress compared to untreated slices from the same mice (untreated: 0.39 [0.35–0.48]; n = 13; D-AP5-treated: 0.32 [0.24–0.42]; n = 17; p = 0.0445; *Figure 4C*). Thus, STN neurons from BACHD mice exhibit elevated mitochondrial oxidant stress, which can be reduced by antagonism of NMDARs.

Impaired autonomous activity of STN neurons in BACHD mice is due to increased activation of K_{ATP} channels

NMDAR receptor-generated mitochondrial oxidant stress in BACHD may lead to the activation of K_{ATP} channels, which act as metabolic sensors and homeostatic regulators of excitability in multiple cell types (*Nichols, 2006*). STN neurons abundantly express all the molecular components of K_{ATP} channels including the Kir6.2 pore-forming subunit of the K_{ATP} channel (*Thomzig et al., 2005*) and the SUR1, SUR2A and SUR2B regulatory subunits (*Karschin et al., 1997*; *Zhou et al., 2012*). To determine whether K_{ATP} channels are responsible for impaired firing in BACHD mice, the effects of the K_{ATP} channel inhibitor glibenclamide (100 nM) on WT and phenotypic BACHD autonomous firing ex vivo were compared. Glibenclamide application increased both the rate (BACHD control: 5.7 [1.4–9.1] Hz; BACHD glibenclamide: 11.3 [9.2–13.3] Hz; n = 15; p = 0.0003) and regularity (BACHD
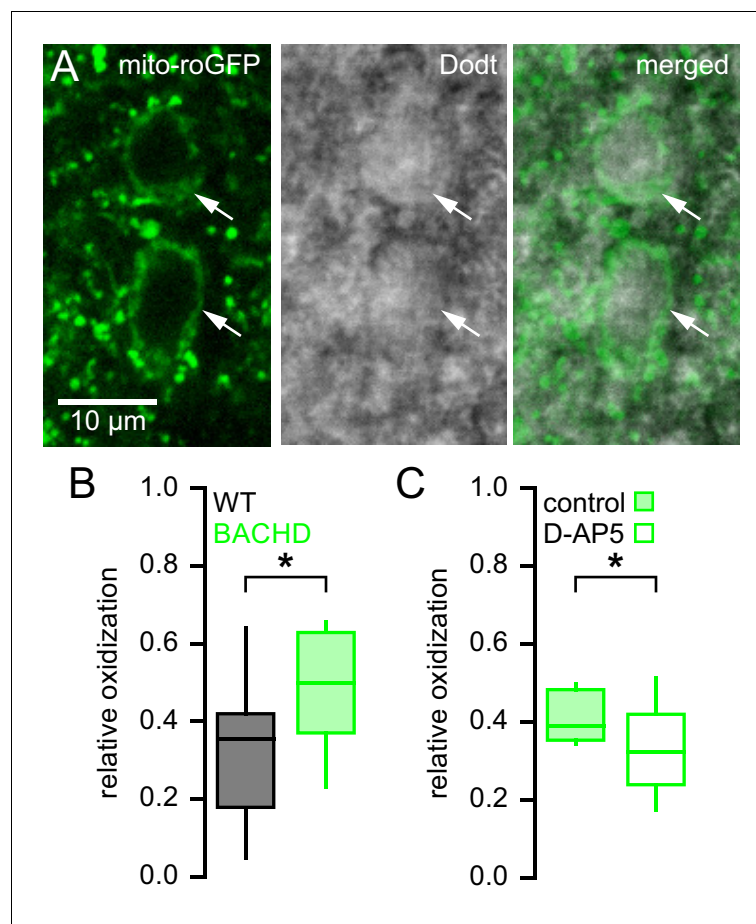
Figure 4. Mitochondrial oxidant stress is elevated in STN neurons from BACHD mice. (A) Two-photon (left), Dodt contrast (center) and combined (right) images showing expression of MTS-roGFP (green) in STN neurons of a BACHD mouse. (B) Population data illustrating greater relative oxidation of mitochondria in BACHD STN neurons compared to WT STN neurons. (C) Population data showing that >3 hr pre-treatment with the NMDA receptor antagonist D-AP5 (50 μM) lowered the relative oxidation of mitochondria in BACHD STN neurons. Arrows indicate MTS-roGFP expressing STN neurons; *p < 0.05. Data for panel B provided in *Figure 4—source data 1*; data for panel C provided in *Figure 4—source data 2*.
DOI: 10.7554/eLife.21616.010

The following source data is available for figure 4:

Source data 1. The relative mitochondrial oxidant stress of WT and BACHD STN neurons in *Figure 4B*.
DOI: 10.7554/eLife.21616.011

Source data 2. The relative mitochondrial oxidant stress of control and D-AP5 pre-treated BACHD STN neurons in *Figure 4C*.
DOI: 10.7554/eLife.21616.012

control CV: 0.41 [0.16–1.43]; BACHD glibenclamide CV: 0.16 [0.12–0.32]; n = 14; p = 0.0001) of autonomous firing in 5–7-month-old BACHD STN neurons (*Figure 5A,B*). In contrast K_{ATP} channel inhibition had no effect on the firing of WT neurons (WT control frequency: 13.2 [8.4–19.6] Hz; WT glibenclamide frequency: 15.7 [9.7–18.4] Hz; n = 8; p = 0.4609; WT control CV: 0.18 [0.11–0.21]; WT glibenclamide CV: 0.14 [0.11–0.19]; n = 8; p = 0.1094).

To further examine the effects of K_{ATP} channels on autonomous firing, whole-cell current clamp recordings were obtained from 5–7-month-old BACHD mice and WT littermates (*Figure 5C,D*). Consistent with the hyperpolarizing and shunting effects of K_{ATP} channels, the interspike voltage trajectory was shallower in BACHD neurons compared to WT (WT: 413.8 [317.1–705.0] mV/s; n = 7; BACHD: 125.3 [59.2–298.0] mV/s; n = 7; p_h = 0.0210). In addition, the rate, regularity and interspike voltage trajectory of autonomous firing of BACHD STN neurons recorded in this configuration
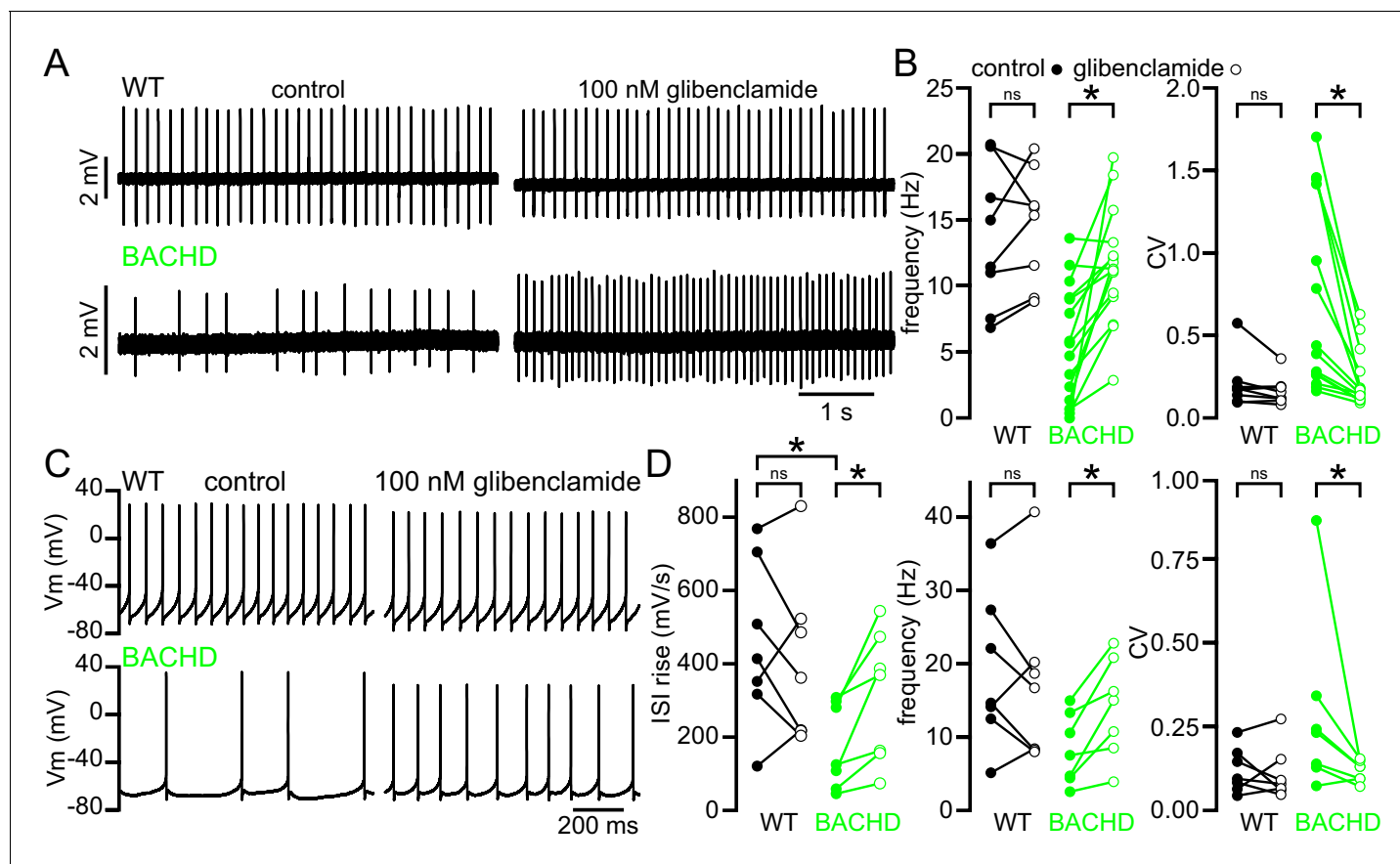
Figure 5. The abnormal autonomous activity of STN neurons in BACHD mice is rescued by inhibition of K_{ATP} channels. (**A**) Examples of loose-seal cell-attached recordings from STN neurons before (left) and after (right) inhibition of K_{ATP} channels with 100 nM glibenclamide. Upper traces show data from a WT mouse; lower traces show data from a BACHD mouse. (**B**) Population data (from 5–7-month-old mice). In WT neurons, inhibition of K_{ATP} channels had mixed effects on firing, whereas in BACHD neurons inhibition of K_{ATP} channels increased both the frequency and regularity of firing. (**C**) Examples of whole-cell recordings from WT and BACHD STN neurons before (left) and after (right) inhibition of K_{ATP} channels with 100 nM glibenclamide. (**D**) Population data (from 5–7-month-old mice). The interspike voltage trajectory was lower in BACHD neurons compared to WT. K_{ATP} channel inhibition increased the interspike voltage trajectory in BACHD neurons but had no effect in WT. As with cell-attached recordings, inhibition of K_{ATP} channels had mixed effects on firing in WT neurons, whereas in BACHD mice inhibition of K_{ATP} channels increased the frequency and regularity of firing. *p < 0.05. ns, not significant. Data for panel B provided in *Figure 5—source data 1*; data for panel D provided in *Figure 5—source data 2*.
DOI: 10.7554/eLife.21616.013

The following source data is available for figure 5:

Source data 1. Autonomous firing frequency and CV for WT and BACHD STN neurons under control conditions and following glibenclamide application in *Figure 5B*.
DOI: 10.7554/eLife.21616.014

Source data 2. Autonomous interspike voltage trajectory, firing frequency and CV for whole-cell recordings from WT and BACHD STN neurons in *Figure 5D*.
DOI: 10.7554/eLife.21616.015

increased following application of glibenclamide (BACHD control frequency: 7.7 [4.5–13.4] Hz; BACHD glibenclamide frequency: 15.1 [8.5–20.9] Hz; n = 7; p = 0.0156; BACHD control CV: 0.24 [0.13–0.35]; BACHD glibenclamide CV: 0.13 [0.10–0.15]; n = 7; p = 0.0313; BACHD control interspike voltage trajectory: 125.3 [59.2–298.0] mV/s; BACHD glibenclamide interspike voltage trajectory: 369.9 [156.7–474.0] mV/s; n = 7; p_h = 0.0313; *Figure 5C,D*). In contrast inhibition of K_{ATP} channels did not alter the firing of WT neurons (WT control frequency: 14.7 [12.5–27.4] Hz; WT glibenclamide frequency: 16.8 [8.3–20.3] Hz; n = 7; p = 0.3750; WT control CV: 0.10 [0.07–0.18]; WT glibenclamide CV: 0.08 [0.06–0.16]; n = 7; p = 0.8125; WT control interspike voltage trajectory: 413.8 [317.1–705.0]

mV/s; n = 7; WT glibenclamide interspike voltage trajectory: 361.9 [216.7–522.9] mV/s; n = 7; p_h = 0.3750; *Figure 5C,D*).

Glibenclamide can also activate Epac2 and Rap1 (*Zhang et al., 2009*), which could rescue firing through a pathway that is independent of K_{ATP} channel inhibition. Therefore, gliclazide, a sulfonylurea that has no effect on Epac2/Rap1 signaling (*Zhang et al., 2009*; *Takahashi et al., 2015*), was applied to STN neurons of 5–7-month-old BACHD mice (*Figure 6*). In loose-seal, cell-attached recordings gliclazide (10 µM) increased both firing rate (control: 5.1 [2.0–8.0] Hz; gliclazide: 9.9 [4.6–13.8] Hz; n = 6; p = 0.0313; *Figure 6*) and regularity (control CV: 0.54 [0.31–0.88]; gliclazide CV: 0.29 [0.10–0.47]; n = 6; p = 0.0313; *Figure 6*) in phenotypic BACHD STN neurons. Together, these data argue that K_{ATP} channels are responsible for the impaired autonomous activity of STN neurons in the BACHD model.

As described above, 3–5 hr NMDAR antagonism with D-AP5 partially rescued autonomous activity in BACHD STN neurons. To determine whether this rescue was mediated through effects on K_{ATP} channels, glibenclamide was applied following this treatment. D-AP5 pre-treatment partially occluded the increases in the autonomous firing rate (BACHD glibenclamide Δ frequency: 4.3 [2.2–8.7] Hz, n = 15; D-AP5 pre-treated BACHD glibenclamide Δ frequency: 1.9 [0.7–3.2] Hz, n = 6; p = 0.0365) and regularity (BACHD glibenclamide Δ CV: −0.25 [−0.85– −0.13], n = 14; D-AP5 pre-treated BACHD glibenclamide Δ CV: −0.09 [−0.10– −0.03], n = 6; p = 0.0154) that accompany K_{ATP} channel inhibition. Thus, these observations are consistent with the conclusion that prolonged NMDAR antagonism partially rescued autonomous activity in BACHD STN neurons through a reduction in K_{ATP} channel-mediated firing disruption.

NMDAR activation produces a persistent K_{ATP} channel-mediated disruption of autonomous activity in WT STN neurons

To further examine whether elevated NMDAR activation can trigger a homeostatic K_{ATP} channel-mediated reduction in autonomous firing in WT STN, brain slices from 2-month-old C57BL/6 mice were incubated in control media or media containing 25 µM NMDA for 1 hr prior to recording (*Figure 7*). NMDA pre-treatment reduced the proportion of autonomously firing neurons (untreated: 66/75 (88%); NMDA: 65/87 (75%); p = 0.0444) and the frequency (untreated: 14.9 [7.8–24.8] Hz; n = 75; NMDA: 5.2 [0.0–14.0] Hz; n = 87; p_h < 0.0001) and regularity (untreated CV: 0.13 [0.08–0.25]; n =

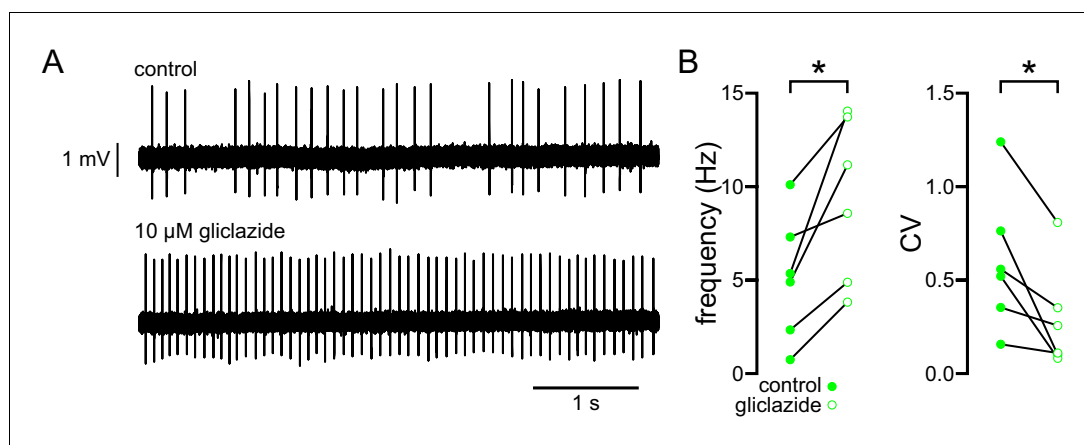**Figure 6.** The abnormal autonomous activity of STN neurons in BACHD mice is rescued by inhibition of K_{ATP} channels with gliclazide. (**A**) Examples of loose-seal cell-attached recordings of a STN neuron from a 6-month-old BACHD mouse before (upper) and after (lower) inhibition of K_{ATP} channels with 10 µM gliclazide. (**B**) Population data (5–7-month-old). In BACHD STN neurons inhibition of K_{ATP} channels with gliclazide increased the frequency and regularity of firing. *p < 0.05. Data for panel **B** provided in *Figure 6—source data 1*.
DOI: 10.7554/eLife.21616.016

The following source data is available for figure 6:

Source data 1. Autonomous firing frequency and CV for WT and BACHD STN neurons under control conditions and following gliclazide application in *Figure 6B*.
DOI: 10.7554/eLife.21616.017

66; NMDA CV: 0.24 [0.10–0.72]; n = 65; p_h = 0.0150; *Figure 7A–C*) of autonomous activity relative to control slices. In a subset of neurons glibenclamide was applied to inhibit K_{ATP} channels. In neurons from untreated slices glibenclamide had no effect on firing rate (control: 16.6 [10.9–31.3] Hz; glibenclamide: 25.0 [16.3–32.8] Hz; n = 6; p_h = 0.2188; *Figure 7A–D*) or regularity (control CV: 0.08 [0.07–0.37]; glibenclamide CV: 0.08 [0.06–0.09]; n = 6; p_h = 0.3125; *Figure 7A–D*). However, in neurons from NMDA pre-treated slices glibenclamide application elevated firing rate (control: 3.3 [2.3–5.1] Hz; glibenclamide: 11.4 [10.8–24.4] Hz; n = 10; p_h = 0.0078; *Figure 7A–D*) and regularity (control CV: 0.83 [0.25–1.03]; glibenclamide CV: 0.12 [0.07–0.16]; n = 8, p_h = 0.0208; *Figure 7A–D*) to levels similar to that seen in untreated slices. Together, these data demonstrate that increased activation of STN NMDARs can lead to a persistent K_{ATP} channel-mediated homeostatic reduction in autonomous activity in STN neurons.
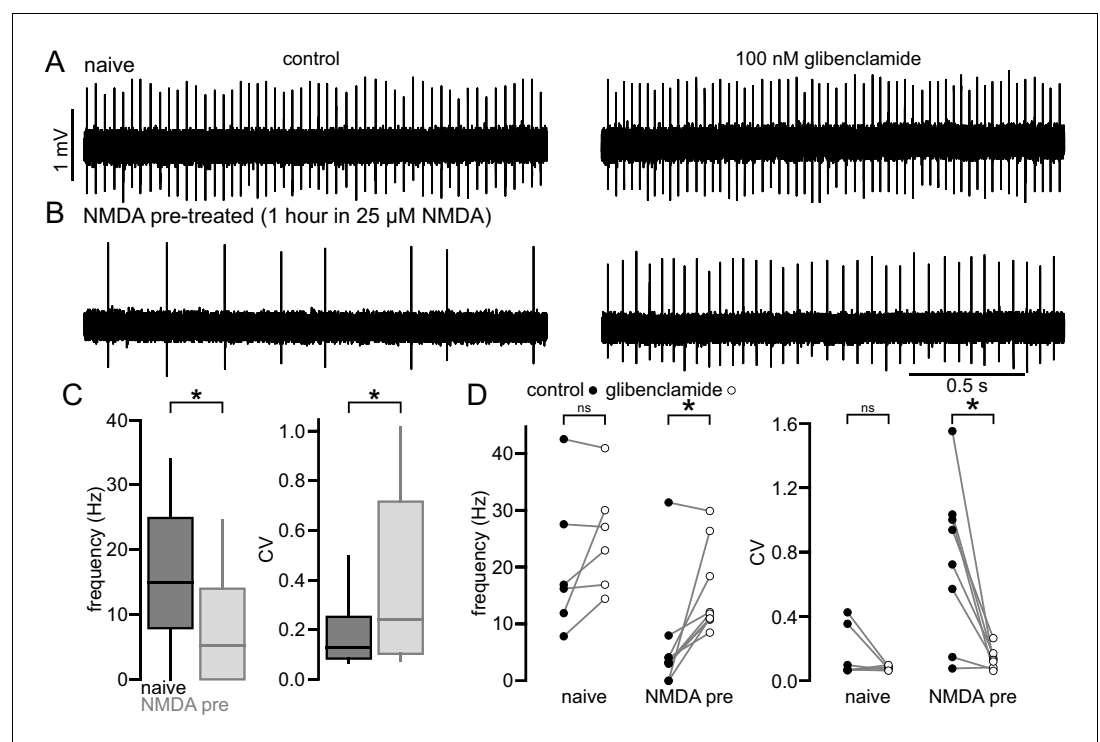
Figure 7. NMDA exposure persistently disrupts autonomous activity. (**A**) Example of a loose-seal cell-attached recording from an STN neuron from an untreated slice from a C57/BL6 mouse before (left) and after (right) inhibition of K_{ATP} channels with 100 nM glibenclamide. (**B**) Example of a loose-seal cell-attached recording from an STN neuron from a slice treated with 25 µM NMDA for 1 hr prior to recording, before (left) and after (right) inhibition of K_{ATP} channels with 100 nM glibenclamide. (**C**) Population data. Following NMDA pre-treatment STN neurons had a lower frequency and regularity of firing. (**D**) Inhibition of K_{ATP} channels with 100 nM glibenclamide restored firing in STN cells from NMDA pre-treated slices but had no effect on firing from naïve slices. *p < 0.05. ns, not significant. Data for panel **C** provided in *Figure 7—source data 1*; data for panel **D** provided in *Figure 7—source data 2*.

The following source data is available for figure 7:

Source data 1. Autonomous firing frequency and CV for control and NMDA pre-treated C57BL/6 STN neurons in *Figure 7C*.
Source data 2. Autonomous firing frequency and CV for control and NMDA pre-treated C57BL/6 STN neurons in control conditions and following glibenclamide application in *Figure 7D*.

Break down of H_2O_2 rescues the firing of BACHD STN neurons to WT levels

Mitochondrial oxidative phosphorylation generates superoxide, which may be dismuted by superoxide dismutase to produce H_2O_2 (*Adam-Vizi, 2005*). Superoxide and hydrogen peroxide can also be produced by NADPH oxidase (*Brennan et al., 2009*). Because K_{ATP} channels are activated by H_2O_2 (*Ichinari et al., 1996*; *Avshalumov et al., 2005*), we tested whether H_2O_2 contributes to K_{ATP} channel-mediated disruption of ex vivo autonomous activity in the BACHD model. The effect of a membrane permeable form of the enzyme catalase (polyethylene glycol-catalase), which breaks down H_2O_2, on the autonomous firing of STN neurons from 4–6-month-old BACHD mice was examined (*Figure 8*). Application of 250 U/ml catalase increased the rate (BACHD control: 3.4 [0.7–5.5] Hz; BACHD catalase: 10.8 [7.6–13.8] Hz; n = 11; p_h = 0.0080; *Figure 8A–C*) and regularity (BACHD control CV: 1.0 [0.3–2.1]; BACHD catalase CV: 0.17 [0.12–0.21]; n = 11; p_h = 0.0060; *Figure 8A–C*) of autonomous firing. Subsequent application of glibenclamide (100 nM) had no additional effect on firing rate (11.8 [8.2–14.4] Hz; n = 11; p_h = 0.9658) or regularity (CV: 0.15 [0.12–0.23]; n = 11; p_h = 0.4922; *Figure 8A–C*). Thus, these results suggest that H_2O_2 underlies K_{ATP} channel activation in BACHD STN neurons.

To test if the actions of H_2O_2 on autonomous firing are confined to its effects on K_{ATP} channels, these experiments were repeated in the presence of glibenclamide. As seen previously, application of glibenclamide increased firing rate (BACHD control: 5.2 [1.0–6.7] Hz; BACHD glibenclamide: 8.5 [7.2–11.6] Hz; n = 8, p_h = 0.0156; *Figure 8D*) and regularity (BACHD control CV: 0.83 [0.27–1.30]; BACHD glibenclamide CV: 0.23 [0.15–0.58]; n = 8; p_h = 0.0156; *Figure 8D*). Subsequent application of catalase had no additional effect on firing rate (8.7 [7.2–14.1] Hz; n = 8; p_h = 0.6406; *Figure 8D*) but did produce a small but statistically significant increase in regularity (CV: 0.14 [0.11–0.21]; n = 8; p_h = 0.0156; *Figure 8D*). In WT mice, catalase application did not change firing rate (WT control: 11.0 [10.5–14.2] Hz; WT catalase: 14.3 [11.3–18.3] Hz; n = 7; p = 0.0781; *Figure 9*) but lead to a small but statistically significant increase in regularity (WT control CV: 0.12 [0.10–0.23]; WT catalase CV: 0.11 [0.07–0.13]; n = 7; p = 0.0469; *Figure 9*). The effects of catalase on the frequency and regularity of firing in BACHD mice were greater than those observed in WT mice (frequency: p = 0.0154; CV: p = 0.0007; *Figure 9*). Together, these data suggest that suppression of autonomous activity of STN neurons in BACHD mice is largely mediated by the modulatory effect of H_2O_2 on K_{ATP} channels.

To test if the elevation of oxidant stress can result in K_{ATP} channel activation in WT STN neurons, glutathione peroxidase was inhibited with mercaptosuccinic acid (MCS) (*Avshalumov et al., 2005*). Following the application of 1 mM MCS both the rate (control: 12.0 [7.8–13.5] Hz; MCS: 9.0 [4.8–10.5] Hz; n = 11; p_h = 0.0068; *Figure 10*) and regularity (control CV: 0.21 [0.15–0.22]; MCS CV: 0.30 [0.22–0.34]; n = 11; p_h = 0.0137) of firing decreased. Subsequent application of glibenclamide rescued both firing rate (14.6 [10.3–19.2] Hz; n = 11; p_h = 0.0020) and regularity (CV: 0.12 [0.12–0.17]; n = 11; p_h = 0.0098; *Figure 10*). These data are also consistent with an action of H_2O_2 on STN K_{ATP} channels.

The STN degenerates progressively in BACHD mice

HD patients exhibit 20–30% STN neuron loss (*Lange et al., 1976*; *Guo et al., 2012*). Because mitochondrial oxidant stress and reactive oxygen species can trigger apoptotic pathways leading to cell death (*Green and Reed, 1998*; *Bossy-Wetzel et al., 2008*), the number of STN neurons in 12-month-old BACHD and WT mice were compared (*Figure 11*). The brains of BACHD mice and WT littermates were first fixed by transcardial perfusion of formaldehyde, sectioned into 70 µm coronal slices and immunohistochemically labeled for neuronal nuclear protein (NeuN). The total number of NeuN-immunoreactive STN neurons and the volume of the STN were then estimated using unbiased stereological techniques. Both the total number of STN neurons (WT: 10,793 [9,070–11,545]; n = 7; BACHD: 7,307 [7,047–9,285]; n = 7; p = 0.0262) and the volume of the STN (WT: 0.087 [0.084–0.095] mm^3; n = 7; BACHD: 0.078 [0.059–0.081] mm^3; n = 7; p = 0.0111; *Figure 11A,B*) were reduced in 12-month-old BACHD versus WT mice. The density of STN neurons was not different in BACHD and WT mice (WT: 121,248 [107,180–126,139] neurons/mm^3; n = 7; BACHD: 115,273 [90,377–135,765] neurons/mm^3; n = 7; p = 0.8048; *Figure 11A,B*). To determine whether the difference in cell number represents an early developmental abnormality or a progressive loss of adult
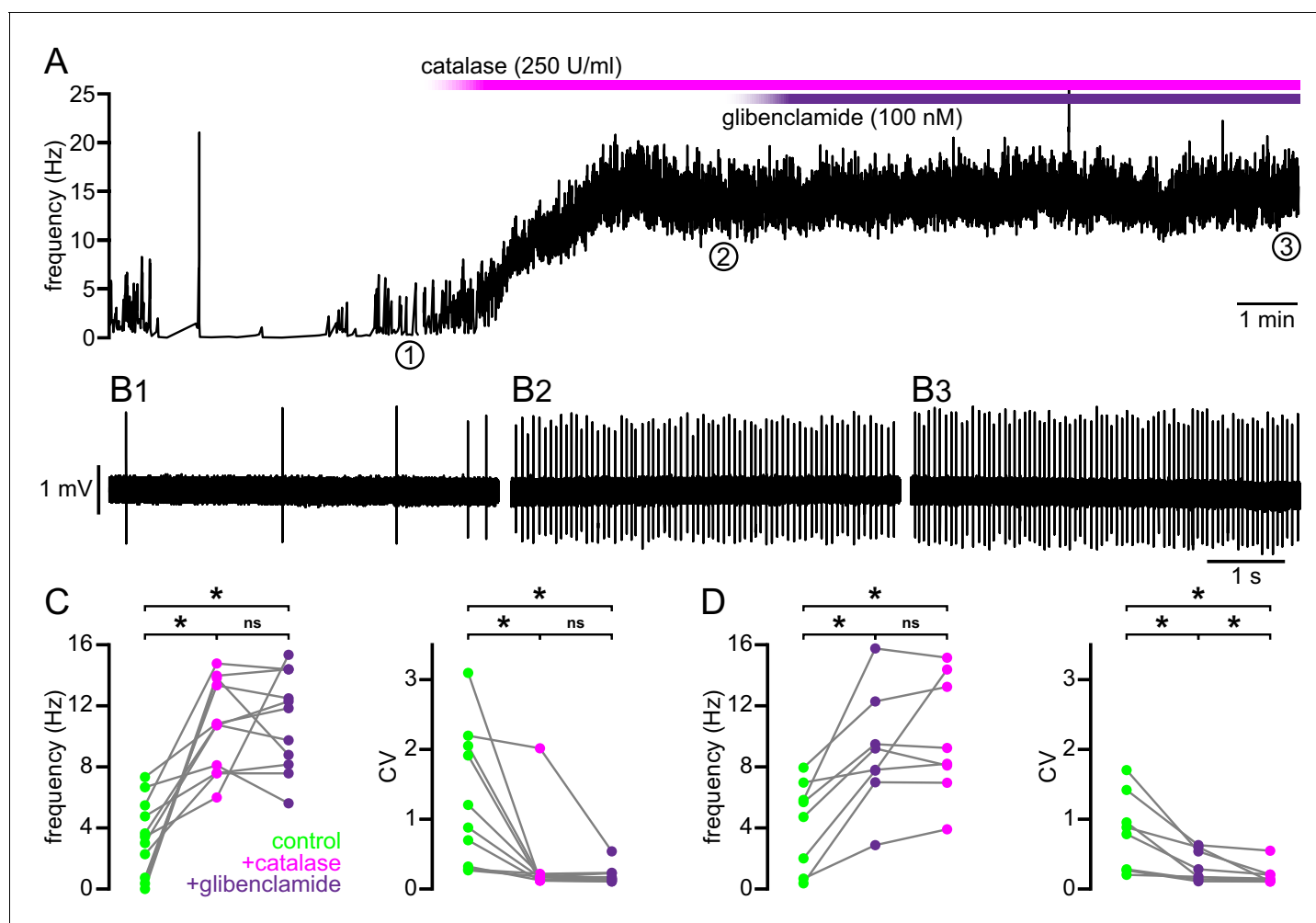
Figure 8. Break down of H_2O_2 by catalase rescues autonomous firing in BACHD STN neurons. (**A**) Example showing the instantaneous firing rate of a BACHD STN neuron in control conditions, during the application of catalase (250 U/ml), and during co-application of catalase and glibenclamide (100 nM). (**B1**) Example of BACHD STN neuron firing in control conditions (marked 1 in **A**). (**B2**) Example of elevated firing during break down of H_2O_2 by catalase (marked 2 in **A**). (**B3**) Example showing no further elevation of firing rate during additional inhibition of K_{ATP} channels with glibenclamide (marked 3 in **A**). (**C**) Population data from 4–6-month old BACHD mice showing an increase in the frequency and regularity of firing following break down of H_2O_2, with no further changes upon K_{ATP} channel inhibition. (**D**) Population data showing an increase in the frequency and regularity of firing following K_{ATP} channel inhibition with no further change in firing rate and a slight increase in firing regularity upon H_2O_2 break down. *p < 0.05. ns, not significant. Data for panels **C**–**D** provided in *Figure 8—source data 1*.

DOI: 10.7554/eLife.21616.021

The following source data is available for figure 8:

Source data 1. Autonomous firing frequency and CV for WT and BACHD STN neurons under control conditions and following catalase and/or glibenclamide application in *Figure 8C–D*.

DOI: 10.7554/eLife.21616.022

neurons, the numbers of neurons in 2-month-old BACHD and WT mice were also compared. At 2-months-old, the total number of STN neurons (WT: 10,373 [9,341–14,414]; n = 7; BACHD: 10,638 [10,513–13,877]; n = 7; p = 0.7104; *Figure 11C*), the volume of the STN (WT: 0.098 [0.090–0.125] mm³; n = 7; BACHD: 0.085 [0.080–0.111] mm³; n = 7; p = 0.1649; *Figure 11C*) and STN neuronal density (106,880 [98,100–115,985] neurons/mm³; n = 7; BACHD: 124,844 [115,479–145,711] neurons/mm³; n = 7; p = 0.1282; *Figure 11C*) were not different in WT and BACHD mice. Together, these data demonstrate that between the ages of 2 months and 12 months BACHD mice lose approximately one third of their STN neurons compared to WT littermates.
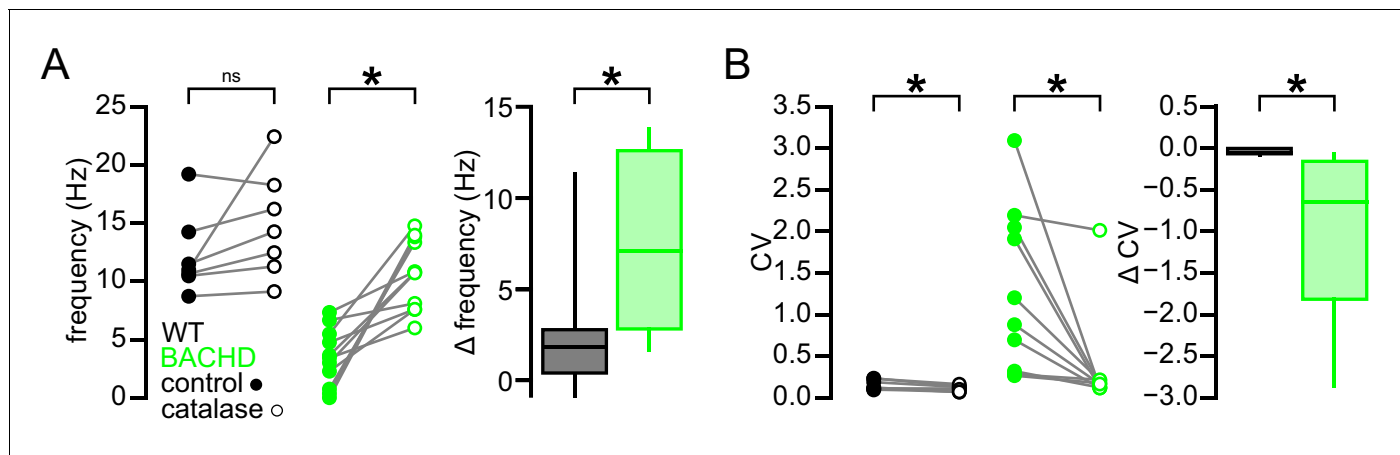
Figure 9. Break down of H_2O_2 by catalase has a relatively minimal effect on autonomous firing in WT STN neurons compared to BACHD neurons. (**A**) Line plots showing of the effect of catalase (250 U/ml) on the frequency of autonomous action potential generation in STN neurons from WT (black) and BACHD mice (green; BACHD data same as in *Figure 8C*). Break down of H_2O_2 elevated autonomous firing in BACHD STN neurons only. The boxplot confirms that the elevation of firing due to catalase application was greater in BACHD mice. (**B**) Line plots illustrating a small but statistically significant effect of catalase on the regularity of autonomous action potential generation in STN neurons from WT mice (black) compared to a larger increase in regularity following catalase application in BACHD neurons (green; BACHD data same as in *Figure 8C*). The boxplot confirms that the increase in regularity due to catalase was greater in BACHD mice. *p < 0.05. ns, not significant. Data provided in *Figure 9—source data 1*.
DOI: 10.7554/eLife.21616.023

The following source data is available for figure 9:

Source data 1. Autonomous firing frequency and CV for WT and BACHD STN neurons under control conditions and following catalase application in *Figure 9*.
DOI: 10.7554/eLife.21616.024

The STN of Q175 KI mice exhibits similar abnormalities to those observed in the BACHD model

STN neurons from BACHD mice exhibit perturbed autonomous firing that is caused by NMDAR activation/signaling leading to mitochondrial oxidant stress, H_2O_2 generation and K_{ATP} channel activation. Furthermore, STN neurons are progressively lost in BACHD mice. To determine whether these features are specific to the BACHD model or a more general feature of HD models, a subset of experiments were repeated in heterozygous Q175 KI mice (*Figure 12*). STN neurons from 6-month-old Q175 mice exhibited a severely reduced rate of autonomous activity (WT: 7.8 [1.9–14.7] Hz; n = 90; Q175: 0.0 [0.0–6.3] Hz; n = 90; p < 0.0001; *Figure 12A,B*), though the regularity of active neurons was unchanged (WT CV: 0.2 [0.1–0.6]; n = 77; Q175 CV: 0.4 [0.1–1.0]; n = 42; p = 0.1506; *Figure 12A,B*). Additionally, there was a large decrease in the proportion of active neurons in the Q175 STN (WT: 77/90 (86%); Q175: 42/90 (47%); p < 0.0001).

Inhibition of K_{ATP} channels with glibenclamide rescued both STN firing rate and regularity in Q175 and increased regularity only in WT (WT control frequency: 9.7 [5.4–13.5] Hz; WT glibenclamide frequency: 10.3 [7.4–15.4] Hz; n = 8; p = 0.1094; Q175 control frequency: 4.8 [3.5–6.2] Hz; Q175 glibenclamide frequency: 11.0 [9.3–13.6] Hz; n = 6; p = 0.0313; WT control CV: 0.19 [0.13–0.47]; WT glibenclamide CV: 0.11 [0.10–0.21]; n = 8; p = 0.0078; Q175 control CV: 0.45 [0.35–0.71]; Q175 glibenclamide CV: 0.15 [0.10–0.17]; n = 6; p = 0.03125; *Figure 12C,D*). Similar to BACHD, Q175 STN neurons recovered to WT-like firing rate following >3 hr pretreatment with D-AP5 (Q175 control: 4.6 [0.0–11.4] Hz; n = 45; Q175 D-AP5 treated: 11.6 [0.0–18.7] Hz; n = 45; p = 0.0144; *Figure 12E,F*), although the regularity (Q175 control CV: 0.16 [0.10–0.66]; n = 15; Q175 D-AP5 treated CV: 0.14 [0.09–0.32]; n = 12; p = 0.2884; *Figure 12E,F*) and proportion of active neurons (Q175 control: 30/45 (67%); Q175 D-AP5 treated: 33/45 (73%); p = 0.6460; *Figure 12E,F*) were unaltered. The 12-month-old Q175 STN (n = 7) exhibited a median 26% reduction in the total number of STN neurons with no effect on other parameters (WT: 8,661 [7,120–9,376] neurons; Q175: 6,420 [5,792–7,024] neurons; p = 0.0111; WT volume: 0.081 [0.074–0.087] mm^3; Q175 volume: 0.079 [0.070–0.091] mm^3; p = 0.6200; WT density: 109,477 [82,180–115,301] neurons/mm^3; Q175 density: 88,968
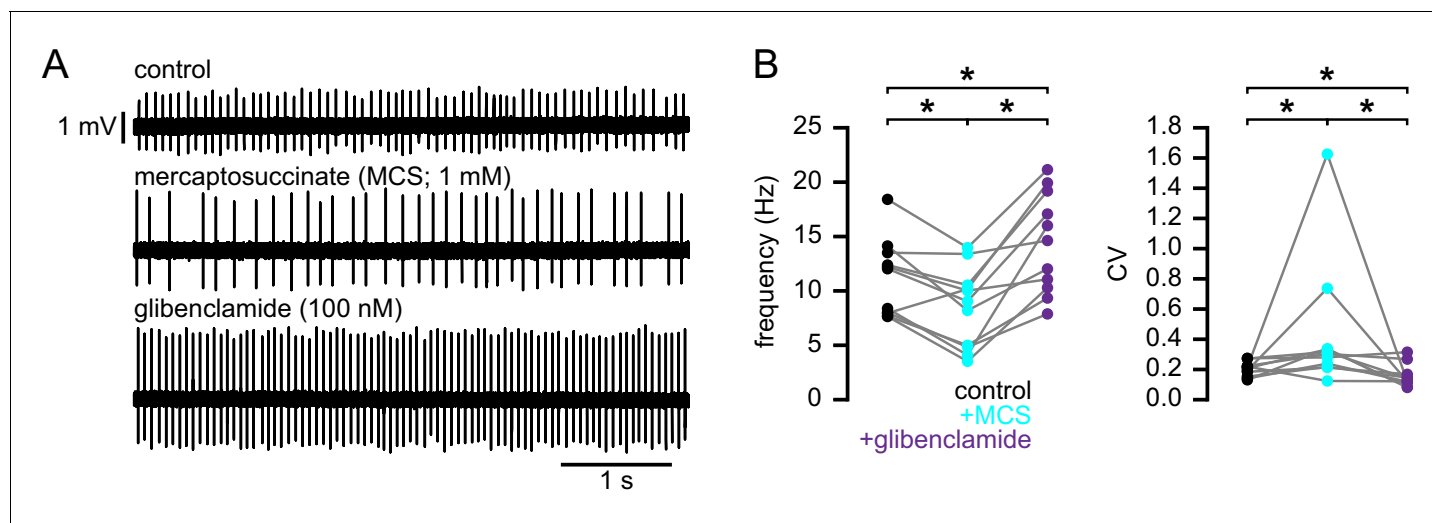
Figure 10. Increasing H_2O_2 levels by inhibition of glutathione peroxidase with mercaptosuccinic acid in WT mice leads to disruption of autonomous action potential generation through activation of K_{ATP} channels. (**A**) Example of autonomous activity of a STN neuron from a C57BL/6 mouse in control conditions (upper), during application of 1 mM mercaptosuccinic acid (MCS; middle), and during subsequent application of 100 nM glibenclamide (lower). These recordings were made in the presence of 20 μM flufenamic acid to block transient receptor potential (TRP) channels (**Lee et al., 2011**). (**B**) Population data showing a decrease in the frequency and regularity of firing following MCS application, which was reversed by subsequent K_{ATP} channel inhibition. *$p < 0.05$. Data for panel **B** provided in **Figure 10—source data 1**.

DOI: 10.7554/eLife.21616.025

The following source data is available for figure 10:

Source data 1. Autonomous firing frequency and CV for WT and BACHD STN neurons under control conditions and following MCS and glibenclamide application in **Figure 10B**.

DOI: 10.7554/eLife.21616.026

[63,624–103,020] neurons/mm³; $p = 0.2086$; **Figure 12G,H**). Taken together, these data show that the STN exhibits similar dysfunction and neuronal loss in both the transgenic BACHD and Q175 KI mouse models of HD.

Discussion

Dysfunction of the striatum and cortex has been extensively characterized in HD models, but relatively few studies have examined the extra-striatal basal ganglia. Here, we report early NMDAR, mitochondrial and firing abnormalities together with progressive loss of STN neurons in two HD mouse models. Furthermore, dysfunction was present in HD mice prior to the onset of major symptoms, implying that it occurs early in the disease process (**Gray et al., 2008**; **Menalled et al., 2012**). Cell death in the STN also preceded that in the striatum, as STN neuronal loss was observed at 12 months of age in both BACHD and Q175 mice, a time point at which striatal neuronal loss is absent but psychomotor dysfunction is manifest (**Gray et al., 2008**; **Heikkinen et al., 2012**; **Smith et al., 2014**; **Mantovani et al., 2016**). Together these findings argue that dysfunction within the STN contributes to the pathogenesis of HD.

Astrocytes appear to play a pivotal role in HD. Expression of mutant huntingtin in astrocytes alone is sufficient to recapitulate neuronal and neurological abnormalities observed in HD and its models (**Bradford et al., 2009**; **Faideau et al., 2010**). Furthermore, astrocyte-specific rescue approaches ameliorate some of the abnormalities observed in HD models (**Tong et al., 2014**; **Oliveira et al., 2016**). In the STN, inhibition of GLT-1 (and GLAST) slowed individual NMDAR EPSCs in WT but not BACHD mice and eliminated the differences in their decay kinetics, arguing that impaired uptake of glutamate by astrocytes contributed to the relative prolongation of NMDAR-mediated EPSCs in BACHD STN neurons. Interestingly, and in contrast to the striatum (**Milnerwood et al., 2010**), when spillover of glutamate onto extrasynaptic receptors was increased by train stimulation and inhibition of astrocytic glutamate uptake, the resulting compound NMDAR EPSC and its prolongation by uptake inhibition were similar in BACHD and WT mice, arguing against
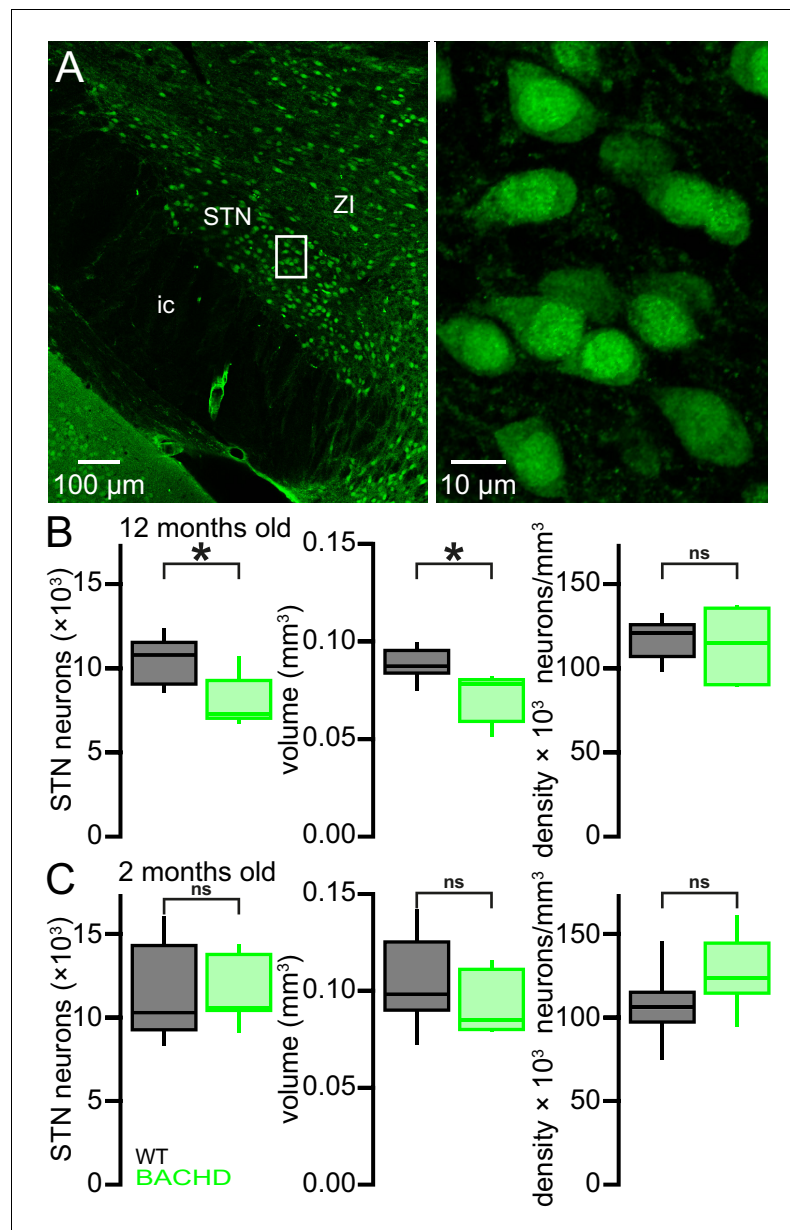
Figure 11. Degeneration of STN neurons in BACHD mice. (**A**) Expression of NeuN in STN neurons in a BACHD mouse (ZI, zone incerta; ic, internal capsule). (**B**) Population data showing a 32.3% reduction in the median STN neuron number and a 10.3% reduction in STN volume at 12 months old. *p < 0.05. ns, not significant. (**C**) Population data showing no difference in STN neuron number, STN volume or density between WT and BACHD mice at 2 months old. Data for panels **B–C** provided in *Figure 11—source data 1*.
DOI: 10.7554/eLife.21616.027

The following source data is available for figure 11:

Source data 1. BACHD STN neuron counts, density and STN volume in *Figure 11B–C*.
DOI: 10.7554/eLife.21616.028

an increase in extrasynaptic STN NMDAR expression/function in BACHD mice. Slowing of astrocytic glutamate uptake has recently been shown to occur during increased presynaptic activity (*Armbruster et al., 2016*). Thus, train stimulation may have slowed glutamate uptake sufficiently to occlude/eliminate the differences in uptake that were observed in BACHD and WT STN neurons during single stimulation. Whether the modest differences in glutamate uptake that
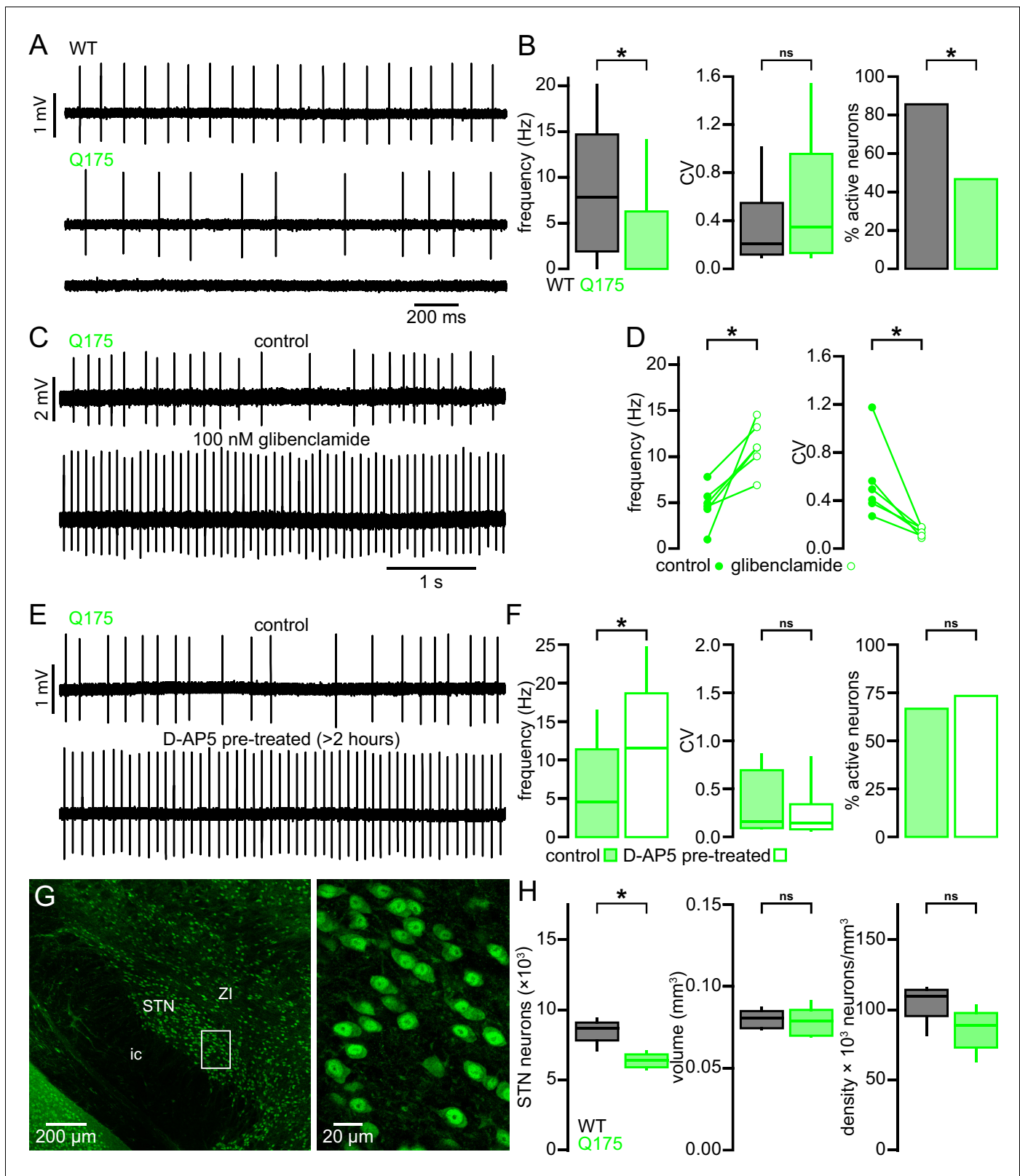
Figure 12. STN neurons exhibit similar dysfunction and degeneration in Q175 mice. (**A**) Examples of impaired (middle, lower) autonomous firing of neurons from Q175 mice relative to WT (upper). (**B**) Population data showing STN neuron firing rate, CV, and proportion of active neurons from 6-month-old WT and Q175 mice. (**C**) Example showing the autonomous firing of a STN neuron from a Q175 mouse before (upper) and during (lower) inhibition of K_{ATP} channels with glibenclamide (100 nM). (**D**) Paired data confirming that inhibition of K_{ATP} channels in Q175 STN neurons consistently

Figure 12 continued on next page

Figure 12 continued

increased the rate (left) and regularity (right) of autonomous firing. (**E**) Examples of autonomous action potential generation from Q175 STN neurons from an untreated slice (upper) and a slice treated with 50 µM D-AP5 for 3–5 hr prior to recording (lower). (**F**) Population data showing STN neuron firing rate, CV, and the proportion of active cells in untreated and D-AP5 treated slices. The frequency of autonomous firing increased in D-AP5 treated slices. (**G**) Expression of NeuN in STN neurons in a Q175 mouse. (**H**) Population data showing STN neuron number (left), STN volume (center), and neuron density (right) in 12-month-old Q175 mice. The number of STN neurons was lower in Q175 mice compared to WT. *p < 0.05. ns, not significant. Data for panel B provided in *Figure 12—source data 1*; data for panel D provided in *Figure 12—source data 2*; data for panel F provided in *Figure 12—source data 3*; data for panel H provided in *Figure 12—source data 4*.

were observed here are sufficient to promote NMDAR-mediated dysfunction in HD STN neurons remains to be determined.

NMDARs play a key role in the abnormal activity of STN neurons in HD models. Antagonism of STN NMDARs in BACHD and Q175 brain slices rescued autonomous STN firing. Conversely, acute activation of STN NMDARs persistently disrupted STN firing in WT brain slices. If the relatively low level of glutamatergic transmission present ex vivo is sufficient to impair firing then this impairment is likely to be more severe in vivo where STN neurons are powerfully patterned by glutamatergic transmission arising from the cortex, thalamus, pedunculopontine nucleus and superior colliculus (reviewed by *Bevan, 2017*). Non-synaptic sources of extracellular glutamate, such as diffusion/release from astrocytes (*Cavelier and Attwell, 2005*; *Lee et al., 2013*) may also contribute to excessive NMDAR activation in HD mice.

Extended antagonism of NMDARs in BACHD slices also reduced mitochondrial oxidant stress in STN neurons. NMDAR activation can elevate ROS through a variety of Ca^{2+}- and nitric oxide-associated signaling pathways and their actions on mitochondria, NADPH oxidase and antioxidant expression (*Dugan et al., 1995*; *Moncada and Bolaños, 2006*; *Brennan et al., 2009*; *Nakamura and Lipton, 2011*; *Valencia et al., 2013*). Although we saw no evidence of basal mitochondrial dysfunction that was not attributable to increased NMDAR function, there is considerable evidence that mutant huntingtin causes transcriptional dysregulation, which leads to defective mitochondrial quality control, an increase in the proportion of defective, ROS generating mitochondria and an increase in opening of the permeability transition pore (*Milakovic and Johnson, 2005*; *Panov et al., 2002*; *Fernandes et al., 2007*; *Song et al., 2011*; *Chaturvedi et al., 2013*; *Johri et al., 2013*; *Martin et al., 2015*). Thus, basal mitochondrial dysfunction could render HD STN neurons especially sensitive to NMDAR-mediated transmission and signaling.

Catalase rapidly restored autonomous firing in the BACHD model, an effect occluded by inhibition of K_{ATP} channels, arguing that H_2O_2, through its action on K_{ATP} channels is the major cause of firing disruption. H_2O_2 can act on K_{ATP} channels by decreasing their sensitivity to ATP (*Ichinari et al., 1996*), reducing the ratio of ATP to ADP (*Krippeit-Drews et al., 1999*), and/or modulating channel gating through a sGC-cGMP-PKG-ROS(H_2O_2)-ERK1/2-calmodulin-CaMKII signaling pathway (*Zhang et al., 2014*). H_2O_2 is likely to directly modulate STN K_{ATP} channels in HD mice because disrupted firing was also observed when STN neurons were recorded in the whole-cell configuration with patch pipettes containing exogenous ATP. Furthermore, H_2O_2 break down rapidly rescued activity, consistent with a direct action on K_{ATP} channels. H_2O_2-dependent modulation of K_{ATP} channels has been extensively characterized in midbrain dopamine neurons where it powerfully suppresses cellular excitability and synaptic transmission (*Avshalumov et al., 2005*; *Bao et al., 2009*). The activation of K_{ATP} channels in STN neurons may represent a form of homeostasis that suppresses firing when mitochondrial oxidant stress is high, limiting the possibility of oxidant damage and bioenergetic failure (*Ray et al., 2012*; *Sena and Chandel, 2012*).

In HD, chronic oxidant stress can lead to damage, such as lipid and protein peroxidation and nuclear/mitochondrial DNA damage, which profoundly impair cellular function and promote cell death (*Perluigi et al., 2005*; *Browne and Beal, 2006*; *Acevedo-Torres et al., 2009*). Consistent with the negative effects of such processes on neuronal viability, we observed progressive loss of STN neurons in both the BACHD and Q175 models. Furthermore, the level of neuronal loss at 12 months in the BACHD and Q175 models was similar to that observed in HD patients (*Lange et al., 1976*; *Guo et al., 2012*). The absence of neuronal loss in the cortex and striatum in the same models at an equivalent time point suggests that STN dysfunction and degeneration may be particularly influential in the early disease process. Although the STN is known to degenerate in HD, it is not clear why neuronal loss is ultimately less than that observed in the striatum at the end stage of the disease, despite the fact that dysfunction and degeneration occur earlier (at least in HD models). Future research will be required to determine whether subtypes of STN neurons exhibit selective vulnerability and/or whether the processes promoting their degeneration, e.g. cortical activation of STN NMDARs, ultimately wane.

As a key component of the hyperdirect and indirect pathways, the STN is critical for constraining cortico-striatal activity underlying action selection (*Albin et al., 1989*; *Oldenburg and Sabatini, 2015*). In the 'classical' model of basal ganglia function, degeneration of indirect pathway striatal projection neurons is proposed to underlie the symptoms of early stage HD (*Albin et al., 1989*). Here we show for the first time that STN dysfunction and neuronal loss precede cortico-striatal abnormalities in HD models. Thus, dysfunction and degeneration of cortical and striatal neurons occurs in concert with profound changes in other elements of the basal ganglia. Therapeutic strategies that target the STN may therefore be useful not only for treating the psychomotor symptoms of early- to mid-stage HD but also for influencing dysfunction and degeneration throughout the cortico-basal ganglia-thalamo-cortical circuit.

Materials and methods

Animals
All animal procedures were performed in accordance with the policies of the Society for Neuroscience and the National Institutes of Health, and approved by the Institutional Animal Care and Use Committee of Northwestern University. Adult male hemizygous BACHD mice (RRID:IMSR_JAX: 008197) and heterozygous Q175 mice (RRID:IMSR_JAX:027410), their WT litter mates, and C57BL/6 mice (Charles River Laboratories International, Inc., Wilmington, MA, USA) were used in this study.

Stereotaxic injection of viral vectors
Mice were anesthetized with 1–2% isoflurane (Smiths Medical ASD, Inc., Dublin, OH, USA). AAV vectors (serotype 9; ~$10^{12–13}$ GC/ml) engineered to express hChR2(H134R)-eYFP under the hSyn promoter (University of Pennsylvania Vector Core, Philadelphia, PA, USA) or MTS-roGFP under the CMV promoter (*Sanchez-Padilla et al., 2014*) were injected under stereotaxic guidance (Neurostar, Tubingen, Germany). In order to express hChR2(H134R)-eYFP, AAV was injected bilaterally into the primary motor cortex (three injections per hemisphere; coordinates relative to bregma: AP, +0.6 mm, + 1.2 mm, and +1.8 mm; ML, + 1.5 mm, and −1.5 mm; DV, −1.0 mm; 0.3 µl per injection). In order to express MTS-roGFP, AAV was injected bilaterally into the STN (coordinates: AP, −2.06 mm; ML, +1.4 mm, and −1.4 mm; DV, −4.5 mm; 0.4 µl per injection). Brain slices were prepared from AAV-injected mice 10–14 days after injection.

Slice preparation
Mice were lightly anesthetized with isoflurane, deeply anesthetized with ketamine/xylazine (87/13 mg/kg i.p.) and then perfused transcardially with ~10 ml of ice-cold sucrose-based artificial cerebrospinal fluid (sACSF) that contained 230 mM sucrose, 2.5 mM KCl, 1.25 mM NaH_2PO_4, 0.5 mM $CaCl_2$, 10 mM $MgSO_4$, 10 mM glucose, and 26 mM $NaHCO_3$ equilibrated with 95% O_2 and 5% CO_2. The brain was removed, immersed in sASCF and 250 µm sagittal slices were cut with a vibratome (VT1200S; Leica Microsystems Inc., IL, USA). Slices were then transferred to a holding chamber, immersed in ACSF that contained 125 mM NaCl, 2.5 mM KCl, 1.25 mM NaH_2PO_4, 2 mM $CaCl_2$, 2 mM $MgSO_4$, 10 mM glucose, 26 mM $NaHCO_3$, 1 mM sodium pyruvate, and 5 µM L-glutathione

equilibrated with 95% O_2 and 5% CO_2, held at 35°C for 30–45 min, then maintained at room temperature.

Recording

Individual brain slices were placed in a recording chamber where they were perfused at 4–5 ml/min with synthetic interstitial fluid (SIF) at 35°C that contained 126 mM NaCl, 3 mM KCl, 1.25 mM NaH_2PO_4, 1.6 mM $CaCl_2$, 1.5 mM $MgSO_4$, 10 mM glucose and 26 mM $NaHCO_3$ equilibrated with 95% O_2 and 5% CO_2. Somatic recordings were obtained under visual guidance (Axioskop FS2, Carl Zeiss, Oberkochen, Germany) using computer-controlled manipulators (Luigs and Neumann, Ratingen, Germany). Loose-seal cell-attached recordings were made using 3–5 MΩ impedance borosilicate glass pipettes (Warner Instruments, Hamden, CT, USA) that were filled with 140 mM NaCl, 23 mM glucose, 15 mM HEPES, 3 mM KCl, 1.5 mM $MgCl_2$, 1.6 mM $CaCl_2$ (pH 7.2 with NaOH, 300–310 mOsm/l). Whole-cell voltage clamp recordings were made using 3–5 MΩ pipettes filled with 135 mM $CsCH_3O_3S$, 10 mM QX-314, 10 mM HEPES, 5 mM phosphocreatine, 3.8 mM NaCl, 2 mM $Mg_{1.5}ATP$, 1 mM $MgCl_2$, 0.4 mM Na_3GTP, 0.1 mM Na_4EGTA (pH 7.2 with CsOH, 290 mOsm/l). Whole-cell current clamp recordings were made using 10–15 MΩ pipettes filled with 130 mM KCH_3SO_4, 3.8 mM NaCl, 1 mM $MgCl_2$, 10 mM HEPES, 5 mM phosphocreatine di(tris) salt, 0.1 mM Na_4EGTA, 0.4 mM Na_3GTP, and 2 mM $Mg_{1.5}ATP$ (pH 7.3 with KOH; 290 mOsm/l). Electrophysiological records were acquired using a computer running Clampex 10 software (Molecular Devices, Palo Alto, CA, USA; RRID:SCR_011323) connected to a Multiclamp 700B amplifier (Molecular Devices) via a Digidata 1322 A digitizer (Molecular Devices). Data were low-pass filtered at 10 kHz and sampled at 50 kHz. Liquid junction potentials of 10 and 9 mV were accounted for in whole-cell voltage clamp and current clamp recordings respectively, and in voltage clamp recordings series resistance and membrane capacitance were corrected online. All recordings of autonomous action potential generation were made in the acute presence of 50 μM D-AP5, 20 μM DNQX, 10 μM GABAzine, and 2 μM CGP 55845 to block synaptic transmission.

Two-photon imaging

MTS-roGFP-expressing neurons were imaged at 890 nm with 76 MHz pulse repetition and ~250 fs pulse duration at the sample plane. Two-photon excitation was provided by a G8 OPSL pumped Mira 900 F laser (Coherent, Santa Clara, CA, USA) and sample power was regulated by a Pockels cell electro-optic modulator (model M350-50-02-BK, Con Optics, Danbury, CT, USA). Images were acquired using an Ultima 2 P system running PrairieView 5 (Bruker Nano Fluorescence Microscopy, Middleton, WI, USA) and a BX51WI microscope (Olympus, Tokyo, Japan) with a 60 × 0.9 NA objective (UIS1 LUMPFL; Olympus). After baseline fluorescence had been measured, the maximum and minimum fluorescence were determined by the application of 2 mM dithiothreitol and then 200 μM aldrithiol-4 to fully reduce and oxidize the tissue, respectively. The relative oxidation at baseline, a measure of oxidative stress, was then calculated (*Sanchez-Padilla et al., 2014*).

Immunohistochemistry and stereology

Mice were lightly anesthetized with isoflurane, deeply anesthetized with ketamine/xylazine (87/13 mg/kg i.p.) and then perfused transcardially with ~5 ml of phosphate buffered saline (PBS) followed by 30 ml of 4% formaldehyde in 0.1 M phosphate buffer (pH 7.4). Brains were removed and post-fixed for 2 hr in 4% formaldehyde, then washed in PBS. Brains were blocked and 70 μm thick coronal sections containing the STN were cut using a vibratome (VT1000S; Leica). Sections were washed in PBS and incubated for 48 hr at 4°C in anti-NeuN (clone A60; MilliporeSigma, Darmstadt, Germany; RRID:AB_2298772) at 1:200 in PBS with 0.2% Triton X-100 (MilliporeSigma) and 2% normal donkey serum. Sections were then washed in PBS and incubated for 90 min at room temperature in Alexa Fluor 488 donkey anti-mouse IgG (1:250; Jackson Immunoresearch, West Grove, PA, USA; RRID:AB_2340846) in 0.2% Triton X-100 and 2% normal donkey serum. Then the sections were washed in PBS and mounted on glass slides in Prolong Gold anti-fade medium (Thermo Fisher Scientific, Waltham, MA, USA).

NeuN labeled sections were imaged using an Axioskop two microscope (Carl Zeiss) with a 100 × 1.3 NA oil immersion objective (Plan-Neofluar 1018–595; Carl Zeiss). Unbiased stereological counting of STN neurons in a single hemisphere was performed using the optical fractionator technique

(*West et al., 1991*) as implemented in Stereo Investigator (MBF Bioscience, Williston, VT, USA; RRID:SCR_002526), using a counting frame of 50 μm × 50 μm × 8 μm and a grid size of 150 μm × 150 μm; all sections containing the STN were used for counting (~8 sections). STN volume was calculated from the sum of the areal extent of the STN on each section multiplied by the section thickness (70 μm). For all individual counts the Gundersen Coefficient of Error (CE) (*Gundersen et al., 1999*) was less than 0.1 (0.080 [0.075–0.090]), and the investigator performing the counting was blinded to the genotype of the mouse.

Drugs

All drugs used in electrophysiology and imaging experiments were diluted to working concentration in SIF and bath applied. D-AP5, CGP 55845, DNQX, GABAzine (SR 95531), NMDA and gliclazide were purchased from Abcam (Cambridge, MA, USA). Glibenclamide, TFB-TBOA and DL-Dithiothreitol were purchased from Tocris Bioscience (Bristol, UK). Catalase (polyethylene glycol-catalase), aldrithiol-4 and MCS were purchased from Sigma-Aldrich (St. Louis, MO, USA).

Data analysis and statistics

Electrophysiological data were analyzed using routines running in Igor Pro 6 and 7 (Wavemetrics, Portland, OR, USA; RRID:SCR_000325) or matplotlib (*Hunter, 2007*; RRID:SCR_008624). The firing rate of STN neurons was calculated from 1 min of recording or 100 action potentials (whichever covered the longer time period). Imaging data were analyzed using FIJI (*Schindelin et al., 2012*; RRID: SCR_002285). Statistical analyses were performed in Prism 5 (GraphPad Software, San Diego, CA, USA; RRID:SCR_002798) or R (http://www.r-project.org/; RRID:SCR_001905, RRID:SCR_000432). In order to make no assumptions about the distribution of the data, non-parametric statistical tests were used, and data are reported as *median [interquartile range]*; outliers were not excluded from the analysis. An α-level of 0.05 was used for two-way statistical comparisons performed with the Mann-Whitney U test for unpaired data (represented with box plots), the Wilcoxon signed rank test for paired data (tilted line segment plots), Fisher's exact test for categorical data (bar plots) or the F-test for linear regression. Where datasets were used in multiple comparisons the p-value was adjusted to maintain the family-wise error rate at 0.05 using the Holm-Bonferroni method (*Holm, 1979*); adjusted p-values are denoted p_h. Box plots show median (central line), interquartile range (box) and 10–90% range (whiskers). For the primary findings reported in the manuscript, sample sizes for Mann-Whitney and Wilcoxon tests were estimated to achieve a minimum of 80% power using formulae described by *Noether (1987)*. The effect sizes used in these power calculations were estimated using data randomly drawn from uniform distributions (runif() function in R stats package). For Mann-Whitney tests, with a 50 percentile change in median between groups X and Y (the interquartile ranges of the groups don't overlap) $P(Y > X) \approx 0.88$ giving an estimation that at least 10 observations per group would be needed to achieve 80% power; for a 25 percentile change (the median of Y falls outside the interquartile range of X) $P(Y > X) \approx 0.72$ and the estimated requirement is at least 27 observations per group. For Wilcoxon tests, if all pairs of observations show the same direction of change, $P(X + X' > 0) = 1$ giving an estimation that at least 10 observations would be needed to achieve 80% power (note though that it is possible to show empirically that 6 observations gives 100% power in this case); if 90% of observations show the same direction of change, $P(X + X' > 0) \approx 0.98$ and the estimated requirement is at least 12 pairs of observations.

Acknowledgements

Additional information

Author contributions

JFA, Designed the experiments, Conducted electrophysiology, imaging, immunohistochemistry and stereology experiments, Analyzed the data, Wrote the manuscript; ELM, Conducted electrophysiology, immunohistochemistry and stereology experiments; MRMM, Conducted immunohistochemistry and stereology experiments; DLW, Conducted imaging experiments; DJS, Designed experiments; MDB, Designed experiments, Conducted electrophysiology experiments, Wrote the manuscript, Directed the project

Author ORCIDs

Mark D Bevan, http://orcid.org/0000-0001-9759-0163

Ethics

Animal experimentation: This study was performed in accordance with the policies of the Society for Neuroscience and the National Institutes of Health. All animals were handled according to approved Institutional Animal Care and Use Committee protocols (IS00001185) of Northwestern University. All procedures were performed under isoflurane or ketamine/xylazine anesthesia, and every effort was made to minimize suffering.

References

Acevedo-Torres K, Berríos L, Rosario N, Dufault V, Skatchkov S, Eaton MJ, Torres-Ramos CA, Ayala-Torres S. 2009. Mitochondrial DNA damage is a hallmark of chemically induced and the R6/2 transgenic model of Huntington's disease. *DNA Repair* 8:126–136. doi: 10.1016/j.dnarep.2008.09.004, PMID: 18935984

Adam-Vizi V. 2005. Production of reactive oxygen species in brain mitochondria: contribution by electron transport chain and non-electron transport chain sources. *Antioxidants & Redox Signaling* 7:1140–1149. doi: 10.1089/ars.2005.7.1140, PMID: 16115017

Albin RL, Young AB, Penney JB. 1989. The functional anatomy of basal ganglia disorders. *Trends in Neurosciences* 12:366–375. doi: 10.1016/0166-2236(89)90074-X, PMID: 2479133

Anderson KE, Marder KS. 2001. An overview of psychiatric symptoms in Huntington's disease. *Current Psychiatry Reports* 3:379–388. doi: 10.1007/s11920-996-0030-2, PMID: 11559474

Armbruster M, Hanson E, Dulla CG. 2016. Glutamate clearance is locally modulated by presynaptic neuronal activity in the cerebral cortex. *Journal of Neuroscience* 36:10404–10415. doi: 10.1523/JNEUROSCI.2066-16.2016, PMID: 27707974

Arzberger T, Krampfl K, Leimgruber S, Weindl A. 1997. Changes of NMDA receptor subunit (NR1, NR2B) and glutamate transporter (GLT1) mRNA expression in Huntington's disease–an in situ hybridization study. *Journal of Neuropathology and Experimental Neurology* 56:440–454. doi: 10.1097/00005072-199704000-00013, PMID: 9100675

Atherton JF, Kitano K, Baufreton J, Fan K, Wokosin D, Tkatch T, Shigemoto R, Surmeier DJ, Bevan MD. 2010. Selective participation of somatodendritic HCN channels in inhibitory but not excitatory synaptic integration in neurons of the subthalamic nucleus. *Journal of Neuroscience* 30:16025–16040. doi: 10.1523/JNEUROSCI.3898-10.2010, PMID: 21106841

Atherton JF, Wokosin DL, Ramanathan S, Bevan MD. 2008. Autonomous initiation and propagation of action potentials in neurons of the subthalamic nucleus. *The Journal of Physiology* **586**:5679–5700. doi: 10.1113/jphysiol.2008.155861, PMID: 18832425

Avshalumov MV, Chen BT, Koós T, Tepper JM, Rice ME. 2005. Endogenous hydrogen peroxide regulates the excitability of midbrain dopamine neurons via ATP-sensitive potassium channels. *Journal of Neuroscience* **25**: 4222–4231. doi: 10.1523/JNEUROSCI.4701-04.2005, PMID: 15858048

Bao L, Avshalumov MV, Patel JC, Lee CR, Miller EW, Chang CJ, Rice ME. 2009. Mitochondria are the source of hydrogen peroxide for dynamic brain-cell signaling. *Journal of Neuroscience* **29**:9002–9010. doi: 10.1523/JNEUROSCI.1706-09.2009, PMID: 19605638

Baunez C, Robbins TW. 1997. Bilateral lesions of the subthalamic nucleus induce multiple deficits in an attentional task in rats. *European Journal of Neuroscience* **9**:2086–2099. doi: 10.1111/j.1460-9568.1997.tb01376.x, PMID: 9421169

Behrens PF, Franz P, Woodman B, Lindenberg KS, Landwehrmeyer GB. 2002. Impaired glutamate transport and glutamate-glutamine cycling: downstream effects of the Huntington mutation. *Brain* **125**:1908–1922. doi: 10.1093/brain/awf180, PMID: 12135980

Beurrier C, Bioulac B, Hammond C. 2000. Slowly inactivating sodium current (I(NaP)) underlies single-spike activity in rat subthalamic neurons. *Journal of Neurophysiology* **83**:1951–1957. PMID: 10758106

Bevan MD. 2017. The subthalamic nucleus. In: Steiner H, Tseng K. Y (Eds). *Handbook of Basal Ganglia Structure and Function*. Amsterdam, Netherlands: Academic Press, Elsevier. p 277–291.

Bevan MD, Wilson CJ. 1999. Mechanisms underlying spontaneous oscillation and rhythmic firing in rat subthalamic neurons. *Journal of Neuroscience* **19**:7617–7628. PMID: 10460267

Bickel S, Alvarez L, Macias R, Pavon N, Leon M, Fernandez C, Houghton DJ, Salazar S, Rodríguez-Oroz MC, Juncos J, Guridi J, Delong M, Obeso JA, Litvan I. 2010. Cognitive and neuropsychiatric effects of subthalamotomy for Parkinson's disease. *Parkinsonism & Related Disorders* **16**:535–539. doi: 10.1016/j.parkreldis.2010.06.008, PMID: 20650671

Bossy-Wetzel E, Petrilli A, Knott AB. 2008. Mutant huntingtin and mitochondrial dysfunction. *Trends in Neurosciences* **31**:609–616. doi: 10.1016/j.tins.2008.09.004, PMID: 18951640

Bradford J, Shin JY, Roberts M, Wang CE, Li XJ, Li S. 2009. Expression of mutant huntingtin in mouse brain astrocytes causes age-dependent neurological symptoms. *PNAS* **106**:22480–22485. doi: 10.1073/pnas.0911503106, PMID: 20018729

Brennan AM, Suh SW, Won SJ, Narasimhan P, Kauppinen TM, Lee H, Edling Y, Chan PH, Swanson RA. 2009. NADPH oxidase is the primary source of superoxide induced by NMDA receptor activation. *Nature Neuroscience* **12**:857–863. doi: 10.1038/nn.2334, PMID: 19503084

Browne SE, Beal MF. 2006. Oxidative damage in Huntington's disease pathogenesis. *Antioxidants & Redox Signaling* **8**:2061–2073. doi: 10.1089/ars.2006.8.2061, PMID: 17034350

Callahan JW, Abercrombie ED. 2015a. Age-dependent alterations in the cortical entrainment of subthalamic nucleus neurons in the YAC128 mouse model of Huntington's disease. *Neurobiology of Disease* **78**:88–99. doi: 10.1016/j.nbd.2015.03.006, PMID: 25772440

Callahan JW, Abercrombie ED. 2015b. Relationship between subthalamic nucleus neuronal activity and electrocorticogram is altered in the R6/2 mouse model of Huntington's disease. *The Journal of Physiology* **593**: 3727–3738. doi: 10.1113/JP270268, PMID: 25952461

Cavelier P, Attwell D. 2005. Tonic release of glutamate by a DIDS-sensitive mechanism in rat hippocampal slices. *The Journal of Physiology* **564**:397–410. doi: 10.1113/jphysiol.2004.082131, PMID: 15695241

Chaturvedi RK, Flint Beal M. 2013. Mitochondrial diseases of the brain. *Free Radical Biology and Medicine* **63**:1–29. doi: 10.1016/j.freeradbiomed.2013.03.018, PMID: 23567191

Chevalier G, Deniau JM. 1990. Disinhibition as a basic process in the expression of striatal functions. *Trends in Neurosciences* **13**:277–280. doi: 10.1016/0166-2236(90)90109-N, PMID: 1695403

Chu HY, Atherton JF, Wokosin D, Surmeier DJ, Bevan MD. 2015. Heterosynaptic regulation of external globus pallidus inputs to the subthalamic nucleus by the motor cortex. *Neuron* **85**:364–376. doi: 10.1016/j.neuron.2014.12.022, PMID: 25578364

Crossman AR, Mitchell IJ, Sambrook MA, Jackson A. 1988. Chorea and myoclonus in the monkey inclued by Gamma-aminobutyric acid Antagonism in the lentiform complex. *Brain* **111**:1211–1233. doi: 10.1093/brain/111.5.1211

Do MT, Bean BP. 2003. Subthreshold sodium currents and pacemaking of subthalamic neurons: modulation by slow inactivation. *Neuron* **39**:109–120. doi: 10.1016/s0896-6273(03)00360-x , PMID: 12848936

Dugan LL, Sensi SL, Canzoniero LM, Handran SD, Rothman SM, Lin TS, Goldberg MP, Choi DW. 1995. Mitochondrial production of reactive oxygen species in cortical neurons following exposure to N-methyl-D-aspartate. *Journal of Neuroscience* **15**:6377–6388. PMID: 7472402

Dvorzhak A, Vagner T, Kirmse K, Grantyn R. 2016. Functional indicators of Glutamate transport in single striatal astrocytes and the influence of Kir4.1 in normal and Huntington mice. *Journal of Neuroscience* **36**:4959–4975. doi: 10.1523/JNEUROSCI.0316-16.2016, PMID: 27147650

Faideau M, Kim J, Cormier K, Gilmore R, Welch M, Auregan G, Dufour N, Guillermier M, Brouillet E, Hantraye P, Déglon N, Ferrante RJ, Bonvento G. 2010. In vivo expression of polyglutamine-expanded huntingtin by mouse striatal astrocytes impairs glutamate transport: a correlation with Huntington's disease subjects. *Human Molecular Genetics* **19**:3053–3067. doi: 10.1093/hmg/ddq212, PMID: 20494921

Fan MM, Raymond LA. 2007. N-methyl-D-aspartate (NMDA) receptor function and excitotoxicity in Huntington's disease. *Progress in Neurobiology* **81**:272–293. doi: 10.1016/j.pneurobio.2006.11.003, PMID: 17188796

Fernandes HB, Baimbridge KG, Church J, Hayden MR, Raymond LA. 2007. Mitochondrial sensitivity and altered calcium handling underlie enhanced NMDA-induced apoptosis in YAC128 model of Huntington's disease. *Journal of Neuroscience* **27**:13614–13623. doi: 10.1523/JNEUROSCI.3455-07.2007, PMID: 18077673

Gray M, Shirasaki DI, Cepeda C, André VM, Wilburn B, Lu XH, Tao J, Yamazaki I, Li SH, Sun YE, Li XJ, Levine MS, Yang XW. 2008. Full-length human mutant huntingtin with a stable polyglutamine repeat can elicit progressive and selective neuropathogenesis in BACHD mice. *Journal of Neuroscience* **28**:6182–6195. doi: 10.1523/JNEUROSCI.0857-08.2008, PMID: 18550760

Green DR, Reed JC. 1998. Mitochondria and apoptosis. *Science* **281**:1309–1312. doi: 10.1126/science.281.5381.1309, PMID: 9721092

Gundersen HJ, Jensen EB, Kiêu K, Nielsen J. 1999. The efficiency of systematic sampling in stereology–reconsidered. *Journal of Microscopy* **193**:199–211. doi: 10.1046/j.1365-2818.1999.00457.x, PMID: 10348656

Guo Z, Rudow G, Pletnikova O, Codispoti KE, Orr BA, Crain BJ, Duan W, Margolis RL, Rosenblatt A, Ross CA, Troncoso JC. 2012. Striatal neuronal loss correlates with clinical motor impairment in Huntington's disease. *Movement Disorders* **27**:1379–1386. doi: 10.1002/mds.25159, PMID: 22975850

Hamada I, DeLong MR. 1992. Excitotoxic acid lesions of the primate subthalamic nucleus result in transient dyskinesias of the contralateral limbs. *Journal of Neurophysiology* **68**:1850–1858. PMID: 1479448

Hanson GT, Aggeler R, Oglesbee D, Cannon M, Capaldi RA, Tsien RY, Remington SJ. 2004. Investigating mitochondrial redox potential with redox-sensitive green fluorescent protein indicators. *Journal of Biological Chemistry* **279**:13044–13053. doi: 10.1074/jbc.M312846200, PMID: 14722062

Heikkinen T, Lehtimäki K, Vartiainen N, Puoliväli J, Hendricks SJ, Glaser JR, Bradaia A, Wadel K, Touller C, Kontkanen O, Yrjänheikki JM, Buisson B, Howland D, Beaumont V, Munoz-Sanjuan I, Park LC. 2012. Characterization of neurophysiological and behavioral changes, MRI brain volumetry and 1H MRS in zQ175 knock-in mouse model of Huntington's disease. *PLoS One* **7**:e50717. doi: 10.1371/journal.pone.0050717, PMID: 23284644

Holm S. 1979. A simple sequentially rejective multiple test procedure. *Scandinavian Journal of Statistics* **6**:65–70. doi: 10.2307/4615733

Huang K, Kang MH, Askew C, Kang R, Sanders SS, Wan J, Davis NG, Hayden MR. 2010. Palmitoylation and function of glial glutamate transporter-1 is reduced in the YAC128 mouse model of Huntington disease. *Neurobiology of Disease* **40**:207–215. doi: 10.1016/j.nbd.2010.05.027, PMID: 20685337

Hunter JD. 2007. Matplotlib: A 2D Graphics environment. *Computing in Science & Engineering* **9**:90–95. doi: 10.1109/MCSE.2007.55

Huntington's Disease Collaborative Research Group. 1993. A novel gene containing a trinucleotide repeat that is expanded and unstable on Huntington's disease chromosomes. *Cell* **72**:971–983. doi: 10.1016/0092-8674(93)90585-e

Ichinari K, Kakei M, Matsuoka T, Nakashima H, Tanaka H. 1996. Direct activation of the ATP-sensitive potassium channel by oxygen free radicals in guinea-pig ventricular cells: its potentiation by MgADP. *Journal of Molecular and Cellular Cardiology* **28**:1867–1877. doi: 10.1006/jmcc.1996.0179, PMID: 8899545

Jahanshahi M, Obeso I, Baunez C, Alegre M, Krack P. 2015. Parkinson's disease, the subthalamic nucleus, inhibition, and impulsivity. *Movement Disorders* **30**:128–140. doi: 10.1002/mds.26049, PMID: 25297382

Jiang R, Diaz-Castro B, Looger LL, Khakh BS. 2016. Dysfunctional calcium and glutamate signaling in striatal astrocytes from Huntington's disease model mice. *Journal of Neuroscience* **36**:3453–3470. doi: 10.1523/JNEUROSCI.3693-15.2016, PMID: 27013675

Johri A, Chandra A, Beal MF. 2013. PGC-1α, mitochondrial dysfunction, and Huntington's disease. *Free Radical Biology and Medicine* **62**:37–46. doi: 10.1016/j.freeradbiomed.2013.04.016, PMID: 23602910

Karschin C, Ecke C, Ashcroft FM, Karschin A. 1997. Overlapping distribution of K(ATP) channel-forming Kir6.2 subunit and the sulfonylurea receptor SUR1 in rodent brain. *FEBS Letters* **401**:59–64. doi: 10.1016/S0014-5793(96)01438-X, PMID: 9003806

Kirkwood SC, Su JL, Conneally P, Foroud T. 2001. Progression of symptoms in the early and middle stages of Huntington disease. *Archives of Neurology* **58**:273–278. doi: 10.1001/archneur.58.2.273, PMID: 11176966

Kita T, Kita H. 2012. The subthalamic nucleus is one of multiple innervation sites for long-range corticofugal axons: a single-axon tracing study in the rat. *Journal of Neuroscience* **32**:5990–5999. doi: 10.1523/JNEUROSCI.5717-11.2012, PMID: 22539859

Kravitz AV, Freeze BS, Parker PR, Kay K, Thwin MT, Deisseroth K, Kreitzer AC. 2010. Regulation of parkinsonian motor behaviours by optogenetic control of basal ganglia circuitry. *Nature* **466**:622–626. doi: 10.1038/nature09159, PMID: 20613723

Kravitz AV, Kreitzer AC. 2012. Striatal mechanisms underlying movement, reinforcement, and punishment. *Physiology* **27**:167–177. doi: 10.1152/physiol.00004.2012, PMID: 22689792

Krippeit-Drews P, Kramer C, Welker S, Lang F, Ammon HP, Drews G. 1999. Interference of H2O2 with stimulus-secretion coupling in mouse pancreatic beta-cells. *The Journal of Physiology* **514**:471–481. doi: 10.1111/j.1469-7793.1999.471ae.x., PMID: 9852328

Lange H, Thörner G, Hopf A, Schröder KF. 1976. Morphometric studies of the neuropathological changes in choreatic diseases. *Journal of the Neurological Sciences* **28**:401–425. doi: 10.1016/0022-510X(76)90114-3, PMID: 133209

Lee CR, Witkovsky P, Rice ME. 2011. Regulation of substantia nigra pars reticulata GABAergic neuron activity by H2O2 via flufenamic Acid- Sensitive Channels and K(ATP) Channels. *Frontiers in Systems Neuroscience* **5**:41–52. doi: 10.3389/fnsys.2011.00014, PMID: 21503158

Lee W, Reyes RC, Gottipati MK, Lewis K, Lesort M, Parpura V, Gray M. 2013. Enhanced Ca(2+)-dependent glutamate release from astrocytes of the BACHD Huntington's disease mouse model. *Neurobiology of Disease* **58**:192–199. doi: 10.1016/j.nbd.2013.06.002, PMID: 23756199

Liévens JC, Woodman B, Mahal A, Spasic-Boscovic O, Samuel D, Kerkerian-Le Goff L, Bates GP. 2001. Impaired glutamate uptake in the R6 Huntington's disease transgenic mice. *Neurobiology of Disease* **8**:807–821. doi: 10. 1006/nbdi.2001.0430, PMID: 11592850

Mantovani S, Gordon R, Li R, Christie DC, Kumar V, Woodruff TM. 2016. Motor deficits associated with Huntington's disease occur in the absence of striatal degeneration in BACHD transgenic mice. *Human Molecular Genetics* **25**:1780–1791. doi: 10.1093/hmg/ddw050, PMID: 26908618

Martin DD, Ladha S, Ehrnhoefer DE, Hayden MR. 2015. Autophagy in Huntington disease and huntingtin in autophagy. *Trends in Neurosciences* **38**:26–35. doi: 10.1016/j.tins.2014.09.003, PMID: 25282404

Maurice N, Deniau JM, Glowinski J, Thierry AM. 1999. Relationships between the prefrontal cortex and the basal ganglia in the rat: physiology of the cortico-nigral circuits. *Journal of Neuroscience* **19**:4674–4681. PMID: 10341265

Menalled LB, Kudwa AE, Miller S, Fitzpatrick J, Watson-Johnson J, Keating N, Ruiz M, Mushlin R, Alosio W, McConnell K, Connor D, Murphy C, Oakeshott S, Kwan M, Beltran J, Ghavami A, Brunner D, Park LC, Ramboz S, Howland D. 2012. Comprehensive behavioral and molecular characterization of a new knock-in mouse model of Huntington's disease: zQ175. *PLoS One* **7**:e49838. doi: 10.1371/journal.pone.0049838, PMID: 23284626

Milakovic T, Johnson GV. 2005. Mitochondrial respiration and ATP production are significantly impaired in striatal cells expressing mutant huntingtin. *Journal of Biological Chemistry* **280**:30773–30782. doi: 10.1074/jbc. M504749200, PMID: 15983033

Miller BR, Dorner JL, Shou M, Sari Y, Barton SJ, Sengelaub DR, Kennedy RT, Rebec GV. 2008. Up-regulation of GLT1 expression increases glutamate uptake and attenuates the Huntington's disease phenotype in the R6/2 mouse. *Neuroscience* **153**:329–337. doi: 10.1016/j.neuroscience.2008.02.004, PMID: 18353560

Milnerwood AJ, Gladding CM, Pouladi MA, Kaufman AM, Hines RM, Boyd JD, Ko RW, Vasuta OC, Graham RK, Hayden MR, Murphy TH, Raymond LA. 2010. Early increase in extrasynaptic NMDA receptor signaling and expression contributes to phenotype onset in Huntington's disease mice. *Neuron* **65**:178–190. doi: 10.1016/j. neuron.2010.01.008, PMID: 20152125

Moncada S, Bolaños JP. 2006. Nitric oxide, cell bioenergetics and neurodegeneration. *Journal of Neurochemistry* **97**:1676–1689. doi: 10.1111/j.1471-4159.2006.03988.x, PMID: 16805776

Nakamura T, Lipton SA. 2011. Redox modulation by S-nitrosylation contributes to protein misfolding, mitochondrial dynamics, and neuronal synaptic damage in neurodegenerative diseases. *Cell Death and Differentiation* **18**:1478–1486. doi: 10.1038/cdd.2011.65, PMID: 21597461

Nichols CG. 2006. KATP channels as molecular sensors of cellular metabolism. *Nature* **440**:470–476. doi: 10. 1038/nature04711, PMID: 16554807

Noether GE. 1987. Sample size determination for some common nonparametric tests. *Journal of the American Statistical Association* **82**:645–647. doi: 10.1080/01621459.1987.10478478

Oldenburg IA, Sabatini BL. 2015. Antagonistic but not symmetric regulation of primary motor cortex by basal Ganglia direct and indirect pathways. *Neuron* **86**:1174–1181. doi: 10.1016/j.neuron.2015.05.008, PMID: 26050037

Oliveira AO, Osmand A, Outeiro TF, Muchowski PJ, Finkbeiner S. 2016. αB-Crystallin overexpression in astrocytes modulates the phenotype of the BACHD mouse model of Huntington's disease. *Human Molecular Genetics* **25**:1677–1689. doi: 10.1093/hmg/ddw028, PMID: 26920069

Panov AV, Gutekunst CA, Leavitt BR, Hayden MR, Burke JR, Strittmatter WJ, Greenamyre JT. 2002. Early mitochondrial calcium defects in Huntington's disease are a direct effect of polyglutamines. *Nature Neuroscience* **5**:731–736. doi: 10.1038/nn884, PMID: 12089530

Parsons MP, Raymond LA. 2014. Extrasynaptic NMDA receptor involvement in central nervous system disorders. *Neuron* **82**:279–293. doi: 10.1016/j.neuron.2014.03.030, PMID: 24742457

Parsons MP, Vanni MP, Woodard CL, Kang R, Murphy TH, Raymond LA. 2016. Real-time imaging of glutamate clearance reveals normal striatal uptake in Huntington disease mouse models. *Nature Communications* **7**: 11251. doi: 10.1038/ncomms11251, PMID: 27052848

Perluigi M, Poon HF, Maragos W, Pierce WM, Klein JB, Calabrese V, Cini C, De Marco C, Butterfield DA. 2005. Proteomic analysis of protein expression and oxidative modification in r6/2 transgenic mice: a model of Huntington disease. *Molecular & Cellular Proteomics* **4**:1849–1861. doi: 10.1074/mcp.M500090-MCP200, PMID: 15968004

Ray PD, Huang BW, Tsuji Y. 2012. Reactive oxygen species (ROS) homeostasis and redox regulation in cellular signaling. *Cellular Signalling* **24**:981–990. doi: 10.1016/j.cellsig.2012.01.008, PMID: 22286106

Sanchez-Padilla J, Guzman JN, Ilijic E, Kondapalli J, Galtieri DJ, Yang B, Schieber S, Oertel W, Wokosin D, Schumacker PT, Surmeier DJ. 2014. Mitochondrial oxidant stress in locus coeruleus is regulated by activity and nitric oxide synthase. *Nature Neuroscience* **17**:832–840. doi: 10.1038/nn.3717, PMID: 24816140

Saudou F, Humbert S. 2016. The biology of Huntingtin. *Neuron* **89**:910–926. doi: 10.1016/j.neuron.2016.02.003, PMID: 26938440

Schindelin J, Arganda-Carreras I, Frise E, Kaynig V, Longair M, Pietzsch T, Preibisch S, Rueden C, Saalfeld S, Schmid B, Tinevez JY, White DJ, Hartenstein V, Eliceiri K, Tomancak P, Cardona A. 2012. Fiji: an open-source platform for biological-image analysis. *Nature Methods* **9**:676–682. doi: 10.1038/nmeth.2019, PMID: 22743772

Sena LA, Chandel NS. 2012. Physiological roles of mitochondrial reactive oxygen species. *Molecular Cell* **48**:158–167. doi: 10.1016/j.molcel.2012.09.025, PMID: 23102266

Smith GA, Rocha EM, McLean JR, Hayes MA, Izen SC, Isacson O, Hallett PJ. 2014. Progressive axonal transport and synaptic protein changes correlate with behavioral and neuropathological abnormalities in the heterozygous Q175 KI mouse model of Huntington's disease. *Human Molecular Genetics* **23**:4510–4527. doi: 10.1093/hmg/ddu166, PMID: 24728190

Song W, Chen J, Petrilli A, Liot G, Klinglmayr E, Zhou Y, Poquiz P, Tjong J, Pouladi MA, Hayden MR, Masliah E, Ellisman M, Rouiller I, Schwarzenbacher R, Bossy B, Perkins G, Bossy-Wetzel E. 2011. Mutant huntingtin binds the mitochondrial fission GTPase dynamin-related protein-1 and increases its enzymatic activity. *Nature Medicine* **17**:377–382. doi: 10.1038/nm.2313, PMID: 21336284

Stack EC, Kubilus JK, Smith K, Cormier K, Del Signore SJ, Guelin E, Ryu H, Hersch SM, Ferrante RJ. 2005. Chronology of behavioral symptoms and neuropathological sequela in R6/2 Huntington's disease transgenic mice. *The Journal of Comparative Neurology* **490**:354–370. doi: 10.1002/cne.20680, PMID: 16127709

Tachibana Y, Kita H, Chiken S, Takada M, Nambu A. 2008. Motor cortical control of internal pallidal activity through glutamatergic and GABAergic inputs in awake monkeys. *European Journal of Neuroscience* **27**:238–253. doi: 10.1111/j.1460-9568.2007.05990.x, PMID: 18093168

Takahashi H, Shibasaki T, Park JH, Hidaka S, Takahashi T, Ono A, Song DK, Seino S. 2015. Role of Epac2A/Rap1 signaling in interplay between incretin and sulfonylurea in insulin secretion. *Diabetes* **64**:1262–1272. doi: 10.2337/db14-0576, PMID: 25315008

Thomzig A, Laube G, Prüss H, Veh RW. 2005. Pore-forming subunits of K-ATP channels, Kir6.1 and Kir6.2, display prominent differences in regional and cellular distribution in the rat brain. *Journal of Comparative Neurology* **484**:313–330. doi: 10.1002/cne.20469, PMID: 15739238

Tong X, Ao Y, Faas GC, Nwaobi SE, Xu J, Haustein MD, Anderson MA, Mody I, Olsen ML, Sofroniew MV, Khakh BS. 2014. Astrocyte Kir4.1 ion channel deficits contribute to neuronal dysfunction in Huntington's disease model mice. *Nature Neuroscience* **17**:694–703. doi: 10.1038/nn.3691, PMID: 24686787

Valencia A, Sapp E, Kimm JS, McClory H, Reeves PB, Alexander J, Ansong KA, Masso N, Frosch MP, Kegel KB, Li X, DiFiglia M. 2013. Elevated NADPH oxidase activity contributes to oxidative stress and cell death in Huntington's disease. *Human Molecular Genetics* **22**:1112–1131. doi: 10.1093/hmg/dds516, PMID: 23223017

West MJ, Slomianka L, Gundersen HJ. 1991. Unbiased stereological estimation of the total number of neurons in thesubdivisions of the rat hippocampus using the optical fractionator. *The Anatomical Record* **231**:482–497. doi: 10.1002/ar.1092310411, PMID: 1793176

Wichmann T, DeLong MR. 1996. Functional and pathophysiological models of the basal ganglia. *Current Opinion in Neurobiology* **6**:751–758. doi: 10.1016/S0959-4388(96)80024-9, PMID: 9000030

Zhang CL, Katoh M, Shibasaki T, Minami K, Sunaga Y, Takahashi H, Yokoi N, Iwasaki M, Miki T, Seino S. 2009. The cAMP sensor Epac2 is a direct target of antidiabetic sulfonylurea drugs. *Science* **325**:607–610. doi: 10.1126/science.1172256, PMID: 19644119

Zhang DM, Chai Y, Erickson JR, Brown JH, Bers DM, Lin YF. 2014. Intracellular signalling mechanism responsible for modulation of sarcolemmal ATP-sensitive potassium channels by nitric oxide in ventricular cardiomyocytes. *The Journal of Physiology* **592**:971–990. doi: 10.1113/jphysiol.2013.264697, PMID: 24277866

Zhou M, He HJ, Tanaka O, Sekiguchi M, Kawahara K, Abe H. 2012. Localization of the ATP-sensitive K(+) channel regulatory subunits SUR2A and SUR2B in the rat brain. *Neuroscience Research* **74**:91–105. doi: 10.1016/j.neures.2012.08.005, PMID: 22960600